Process of a Random Planar Quadrangulation

Emily Ewers

Master's thesis
2024:E21

Lund University

Faculty of Science
Centre for Mathematical Sciences
Mathematical Statistics

Centrum Scientiarum Mathematicarum

Abstract

A process of a random graph, that grows in a box $[0, N]^2 \subset \mathbb{R}^2$ and yields a quadrangulation when it stops growing, is investigated in this work. The random components in this model come from the Poisson distributed number of points, the position of those, and the either horizontal or vertical direction in which lines grow from these points. The model finds inspiration in a cellular automata model by Ekström and Turova (2022), which is used to model neuronal activity in the brain. This work provides results on the quadrangulation model, including tail bounds for the distribution of the growth of lines, bounds for the expected values of a model characteristic and the covariance structures of the behaviour around points depending on their distance. It is also set into relation with work on Gilbert tessellation.

Acknowledgements

First, I would like to thank my supervisor Tatyana Turova for all her time, availability, and enthusiasm about this project. I have learnt a lot mathematically and to keep pushing even when progress seems out of reach. I would also like to thank Henrik Ekström, who was a great partner for discussions around these models and who provided me with an algorithm that made the simulations of the process much easier. Last but not least, thank you to my friends and family, who supported me during this work. Special thanks to Svenja Jedhoff and Eric Knop, who gave me valuable feedback on my writing, and to Henrik Bengtsson for our many little discussions around probability theory, often inspired by this thesis.

Contents

1 Introduction

The process of a random quadrangulation treated in this work is inspired by a model for neuronal activity in the brain within a cellular automata setup presented by Ekström and Turova (2022) in [4], described in more detail in Section 3.1. For the original model, different types of behaviours can be characterised. The model presented here is a simplified and approximate version of the behaviour of a model with monotone growth (in time-scale) of the activation set ([4], Model (a) in 3.6), which is defined on $\mathbb{Z}^2$. This work focuses on a modified version in $\mathbb{R}^2$. An example of the quadrangulation is shown in Figure 1. For a specific type of configuration of parameters in the original model, the results presented here can be seen as approximate results on the original model as well.

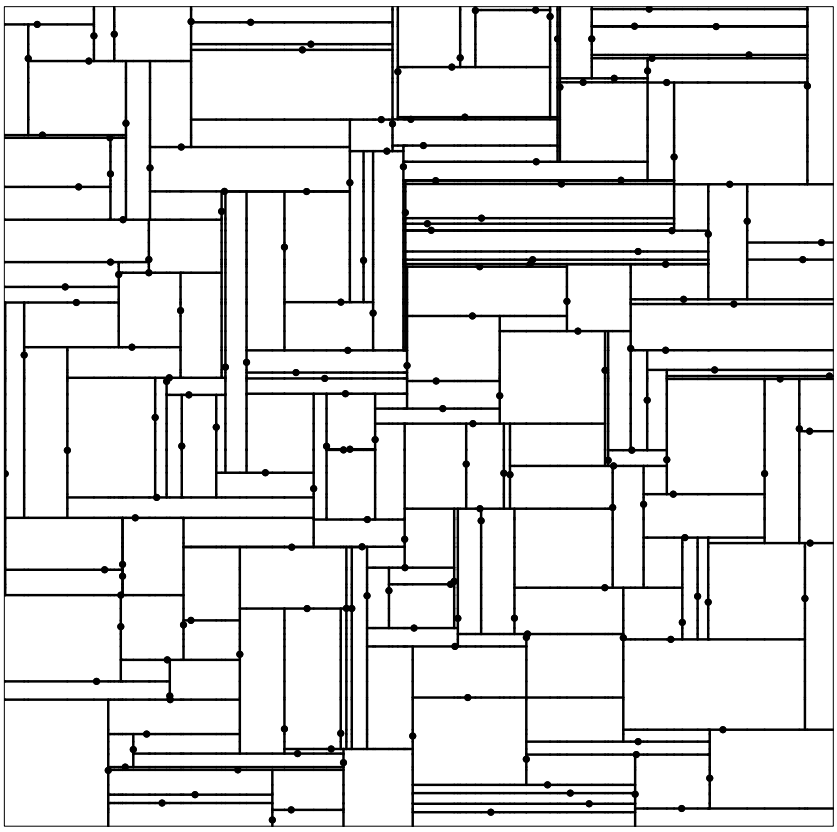

Figure 1: Example of a random quadrangulation that is obtained from the model in $\mathbb{R}^2$ presented in this work.

This problem can partly be categorised within the field of percolation, where the first model was formulated in 1957 ([8], Chapter 1.1). The idea of percolation models is inspired by phenomena in nature and natural sciences, like the spread of water in a porous stone or the spread of a disease in an epidemic. Mathematically, such models are often formulated on the lattices $\mathbb{Z}^d$, but can be generalised to other lattices or graphs. It is explored how and if vertices are connected (through edges) in a stochastic setting. One commonly posed question revolves around the existence of infinite clusters, which often

has a behaviour characterised by different phases and a critical point for a parameter that marks the point of phase transition. Such a phenomenon of change in behaviour at a critical point is also explored in this work.

However, for various forthcoming questions in this work, typical techniques from percolation are not directly applicable because of the time- and spatial dependence and non-monotonicity in some regards. This partly stems from the fact that the cellular automata model arises from a bootstrap percolation with additional activation rules, increasing the degree of complexity and thus preventing common percolation techniques to be applicable. The key idea for this model often lies in reducing the dependence structures sufficiently to find bounds for properties of interest.

Only after deriving the results presented in this work (up to Section 5) did the author become aware of publications on the model presented here. To the author's best knowledge, there are three papers [1], [2], [12] which present approximate results on characteristics of this model, but no exact results were obtained in those works. Our model can be considered as a special case of a tessellation called *Gilbert Tessellation* that dates back to a publication by Gilbert in 1967 [7]. This special case is called *Rectangular Gilbert Tessellation*. The results from [1], [2], [12] are summarised and discussed in relation to our work at the end, as the presented results here are all derived independently. Additionally, our results are of a different type. The language used to describe presented phenomena also differs from the language used in the other publications.

Since our model was derived from the cellular automata model and the authors of [12] derived it from a more general tessellation model, two different backgrounds led to the same model independent of the other. This shows that this model is truly versatile and of mathematical interest.

After introducing some preliminary theory in the next section, the model is illustrated with some examples and first observations in Section 3 to gain intuition for the succeeding results. These are stated and proved in Section 4 and split into the main model of this work and some adjusted versions. Section 5 explores some more properties and generalisations of this model. Finally, Section 6 discusses the results known to the author about rectangular Gilbert tessellation and concludes with open questions.

2 Preliminaries

In this section, some preliminary theory is explained to make the result section more accessible. This includes some results from basic probability theory to remind the reader as well as some tail bounds used to obtain the later presented results.

Two well-known results from basic probability theory are the Law of Total Probability and Law of Total Expectation. To that end, let $(\Omega, \mathcal{F}, \mathbb{P})$ be a probability space and let V be an event on $(\Omega, \mathcal{F}, \mathbb{P})$. The Law of Total Probability is stated here for the discrete

and continuous case in no more generality than needed for this work. Let $\{U_k\}_k$ be a partition of Ω.

(a) **Discrete case:**
$$\mathbb{P}(V) = \sum_k \mathbb{P}(V|U_k)\mathbb{P}(U_k). \tag{1}$$

(b) **Continuous case:** Let X be a random variable on the given probability space with probability density function f. Then:
$$\mathbb{P}(V) = \int_{-\infty}^{\infty} \mathbb{P}(V|X = x)f(x)dx. \tag{2}$$

Let X be a random variable on the probability space $(\Omega, \mathcal{F}, \mathbb{P})$ with existing expected value and let Y be a random variable on the same probability space. Then the Law of Total Expectation states $\mathbb{E}(X) = \mathbb{E}(\mathbb{E}(X|Y))$. Additionally, the following special case holds:
$$\mathbb{E}(X) = \sum_k \mathbb{E}(X|U_k)\mathbb{P}(U_k). \tag{3}$$

The Poisson distribution and process with their properties defined next play a central role in this work.

Definition 2.1 (Poisson Distribution)**.** *([11], Chapter 1.1)*
Let K be a random variable and $\lambda > 0$ the intensity parameter. K is said to have a Poisson distribution $Poi(\lambda)$ if for all $k \in \mathbb{N}_0$:
$$\mathbb{P}(K = k) = \frac{e^{-\lambda}\lambda^k}{k!}. \tag{4}$$
Furthermore it holds that $\mathbb{E}(K) = Var(K) = \lambda$.

Definition 2.2 (Poisson Process)**.** *([3], Chapter 2.3.1)*
Let $\lambda > 0$ be a constant intensity, $\mathbb{R}^d$ the state space, ν_d the Borel measure in $\mathbb{R}^d$ and A a bounded Borel set. A homogeneous Poisson process K, from now on just Poisson process, *is characterised by the following two properties:*

(i) The random number of points $K(A)$ in A has Poisson distribution with expected value $\lambda\nu_d(A)$, in short $K(A) \sim Poi(\lambda\nu_d(A))$.

(ii) For disjoint bounded Borel sets $A_1, \ldots, A_k$, the random variables $K(A_1), \ldots, K(A_k)$ are independent.

The second property is often referred to as independent increments. For such a Poisson process, it holds that, for a compact set A and conditioned on $K(A) = n$, the n points are uniformly distributed in A ([3], Property 2.3.1(e)).

A slightly altered version of a Poisson distribution is the zero-truncated Poisson distribution, allowing only positive integer values. It is derived by taking a Poisson variable and conditioning on it being strictly positive.

Definition 2.3 (Zero-truncated Poisson Distribution)**.** *The random variable K is said to have a zero-truncated Poisson distribution with intensity $\lambda > 0$, in short $K \sim PoiTr(\lambda)$, if the probability mass function is as follows for $k \in \mathbb{N}$:*

$$f_K(k) = \frac{1}{e^\lambda - 1} \cdot \frac{\lambda^i}{i!}. \tag{5}$$

Then the cumulative distribution function is non-zero for $k \geq 1$ and given by

$$F_K(k) = \frac{\sum_{i=0}^{\lfloor k \rfloor} \frac{\lambda^i}{i!} - 1}{e^\lambda - 1}. \tag{6}$$

The next two theorems present bounds for tail probabilities for the Poisson and Binomial distribution, where the first one is a so-called Chernoff bound.

Theorem 2.1. *([10], Section 18.4)*
Let $K \sim Poi(\lambda), \lambda > 0$. Let $x > \lambda$. Then:

$$\mathbb{P}(X \geq x) \leq \exp(x - \lambda) \left(\frac{\lambda}{x}\right)^x. \tag{7}$$

Theorem 2.2. *([13], Theorem 4.5)*
Let $\xi \sim Bin(n, p)$ and denote $\mu = \mathbb{E}(\xi) = np$. Let $\vartheta \in (0, 1)$. Then:

$$\mathbb{P}\left(\xi \leq (1 - \vartheta)\mu\right) \leq \exp\left(-\frac{\vartheta^2 \mu}{2}\right). \tag{8}$$

Let us recall the probability generating function $g_\xi(t)$ for a Binomial random variable $\xi \sim \text{Bin}(n, p)$ with $p \in (0, 1)$ and $q = 1 - p$ for $t \geq 0$ ([9], Chapter 2, p. 61):

$$g_\xi(t) = (q + pt)^n. \tag{9}$$

Finally, we need the concept of first-order stochastic dominance.

Definition 2.4. *([15], Section 4.3)*
Let X and Y be two random variables on some probability space. X is said to (first-order) stochastically dominate Y if for all z:

$$\mathbb{P}(X \geq z) \geq \mathbb{P}(Y \geq z). \tag{10}$$

Equivalently, this is sometimes characterised by $\mathbb{P}(X \leq z) \leq \mathbb{P}(Y \leq z)$, as this can be perceived as more intuitive.

3 The Model

Consider a two-dimensional Poisson process with constant intensity parameter $\lambda > 0$ on $[0, N] \times [0, N]$ in $\mathbb{R}^2$, $N > 0$, i.e., $K \sim \text{Poi}(\lambda N^2)$. Given a realisation of this process, from each point, a line grows with equal probability in either both horizontal or both vertical directions at unit speed. We call this the orientation of a point. A line stops growing if it runs into another one or when it reaches the border of the box. By the time all lines stop growing, which is after at most N time units, all areas separated by the grown lines are almost surely rectangles. Thus, we call this process a quadrangulation. Figure 2 illustrates the process for four vertices.

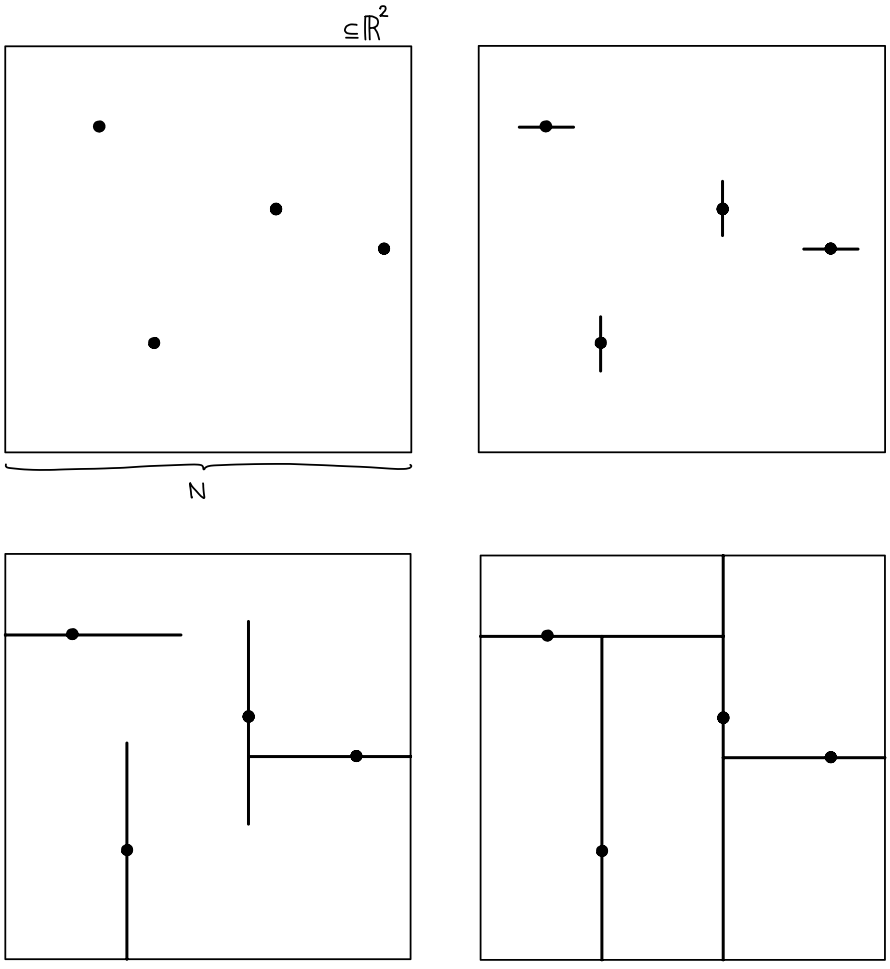

Figure 2: Example of a process with four vertices at time points $t = 0$ in the top left, some $t_1 > 0$ in the top right, the time point $t_2 > t_1$ at the time of the first collision in the bottom left and $t = N$ in the bottom right.

Figures 3 to 7 show examples of realisations of the quadrangulation for 10, 100 and 1000 points. The red points correspond to horizontal and the green ones to vertical lines. We can observe that the exact realisations can look very different for the same number of points. Consider the examples with 10 points first. Observe that in Figure 3, there are

more collisions between lines from points and less lines reaching the border than in the other example with 10 points in Figure 4.

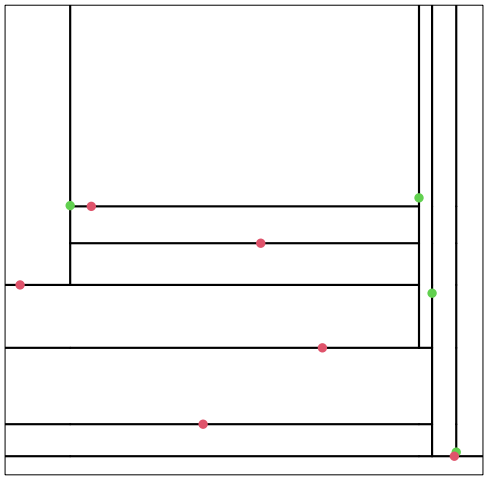

Figure 3: Example (a) with 10 points.

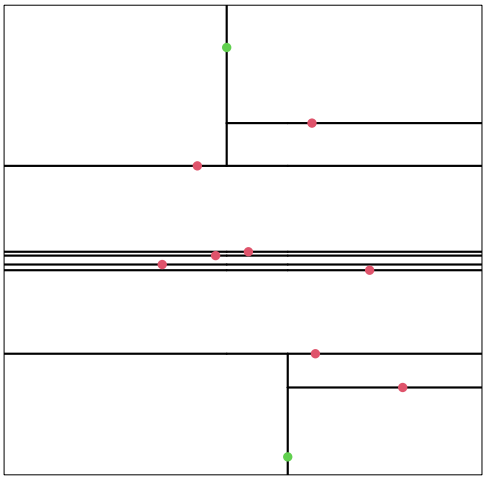

Figure 4: Example (b) with 10 points.

Adding more points, e.g., see Figures 5 and 6 with 100 points, it becomes much less likely that the lines from one vertex both reach the border on opposite sides. The average length of the lines in relation to the size of the box becomes shorter. Furthermore, clusters of rather long parallel lines can be observed. If a point is surrounded by many points with the same orientation, there are less lines that can potentially block its line and more lines that can stop orthogonal lines from cutting it off, making it more likely to grow far.

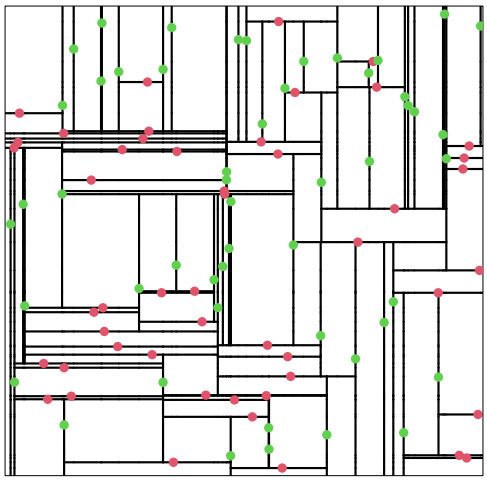

Figure 5: Example (a) with 100 points.

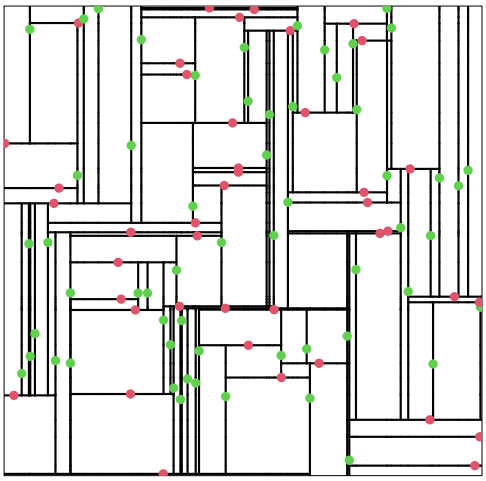

Figure 6: Example (b) with 100 points.

Let us consider even more points, e.g., 1000 points in Figure 7. We can observe that most lines are cut off so quickly that areas far away from each other, for example close

to the upper left and the bottom right corner, do not seem likely to interfere. This phenomenon is considered by deriving covariance results. Moreover, the clusters of very narrow rectangles with parallel longer sides can be observed here, too, separated by groups of rectangles with side lengths similar to each other, in other words, more "square shaped".

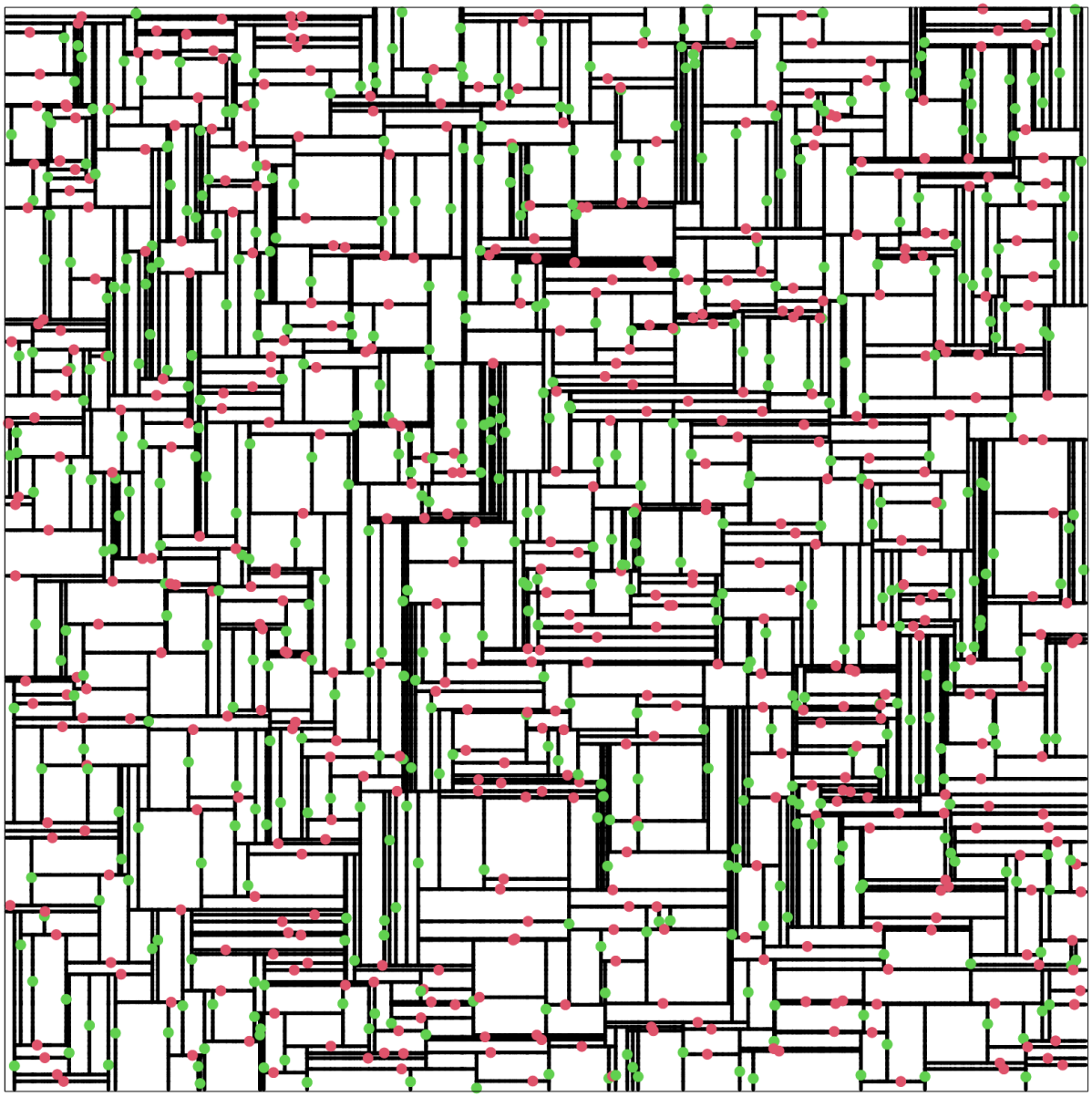

Figure 7: Example with 1000 points.

3.1 Relation to the Cellular Automata Model

The original version of this model is defined on $\mathbb{Z}^2$ in [4]. The growing lines in our model represent the propagation of activation initiated in a random set, which is the counterpart to the Poisson process here. The activation set in [4] is defined by assigning each vertex in $[0, 1, \ldots, N]^2 \subset \mathbb{Z}^2$ the state *active* with probability $p \in (0, 1)$ independently. The rules

for vertices to become active are not described in detail here, but essentially the structure of the active set grows like the lines described in the previous subsection with our model. The rows of active vertices form the shapes of lines, as seen in Figure 8, but the active set remains a countable set of vertices. Note that in addition, both lines stop in case they arrive at the place of collision at the same time (call it head-on collision). Moreover, there is some different behaviour if they run very closely to each other when parallel, which is also disregarded in more detail here. Figure 8 shows an example of a limit pattern for the original model, where we can see the structural similarity to the model in continuous space.

In our model, i.e., on $\Omega \subset \mathbb{R}^2$, the event of a head-on collision has probability 0. Note also that even in the discrete space case, with a very small p, i.e., the points are sparsely spread, the probability of a head-on collision becomes small. So the two models' behaviours are more similar. However, the probability for a head-on collision remains strictly positive for a finite box on $\mathbb{Z}^2$.

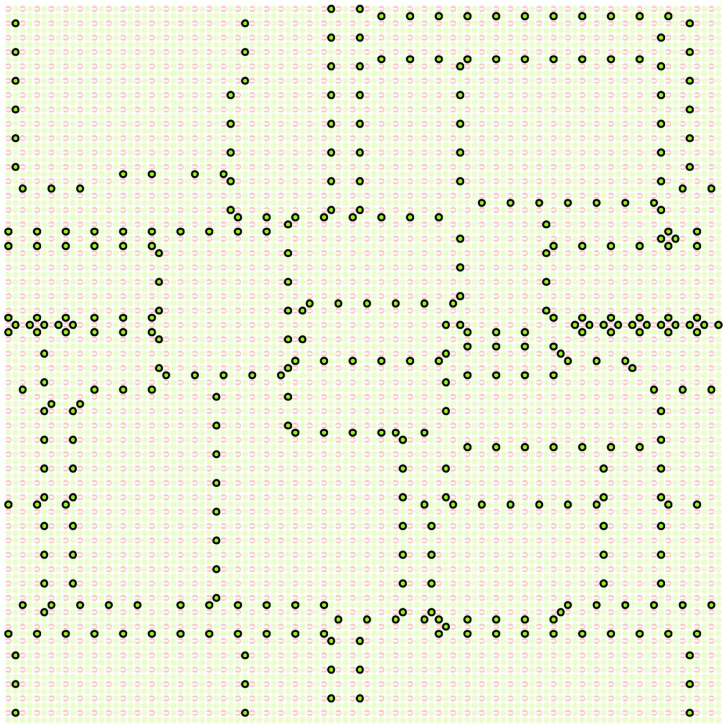

Figure 8: Example of a limit pattern for the corresponding model in the cellular automata with $p = 0.01$, taken from Figure 13 in [4].

The head-on collisions can form patterns that enclose areas in a way that has probability 0 in $\mathbb{R}^2$. Namely, the discrete model does not necessarily result in a quadrangulation. Some examples of possible patterns are shown in Figure 9, where the formed lines are displayed instead of the set of active vertices. The first row shows three examples how the lines can enclose areas entirely (lock-ups) and the second row shows examples of finished processes. While these are mathematically highly interesting to analyse, they also

complicate the behaviour and thus make it more involved to derive any kind of results. Assuming continuous space allows for some simplifications, which help to obtain the results presented in this work.

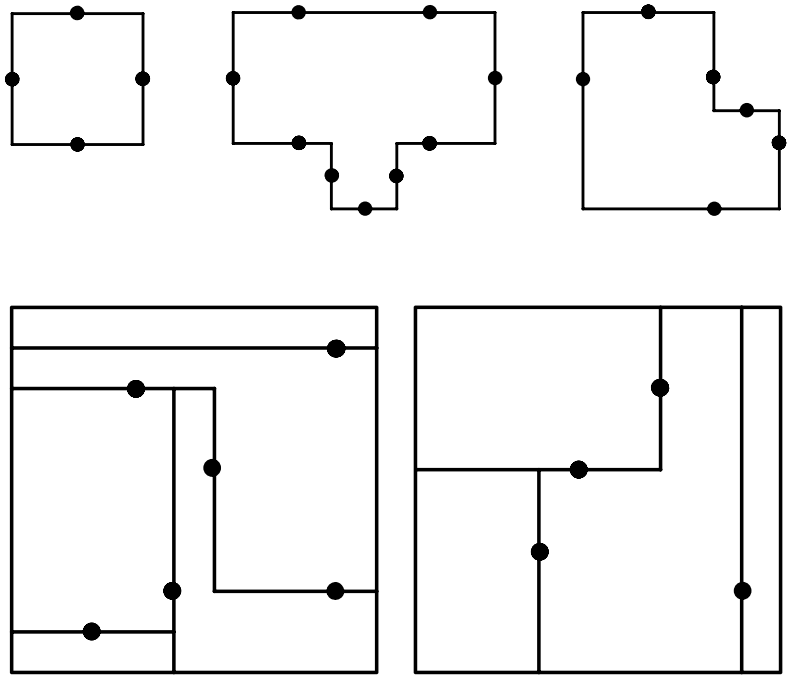

Figure 9: Examples of lock-ups and head-on collisions in a quadrangulation on $\mathbb{Z}^2$.

3.2 Graphical Representation of Dependence Structures

Let us make sure to understand the complexity of the model and its dependence structures by considering some examples. Figure 10 shows how the outcome of the random quadrangulation can change when only one more point is added or a point's orientation is changed and the rest is kept the same. This is because of the chain reactions, which can be started by these changes. In the figure, the first column shows examples of quadrangulations with 5 (A) and 6 (B) points. In the second column, one point is added in each example, while in the third column, the orientation of one point is changed. The added/changed vertex and its line are coloured blue. We can see that the outcomes are strongly influenced by these small changes.

Figure 10 also shows that adding one point does not guarantee a longer total line length, neither does it guarantee the opposite, which gives a non-monotonicity in that regard.

It is also possible to gain intuition for the behaviour of the complexity on a small scale when fixing the number of points to $k = 3$. Up to rotation and flipping, there are five different patterns which the quadrangulation can result in. These are presented in Figure

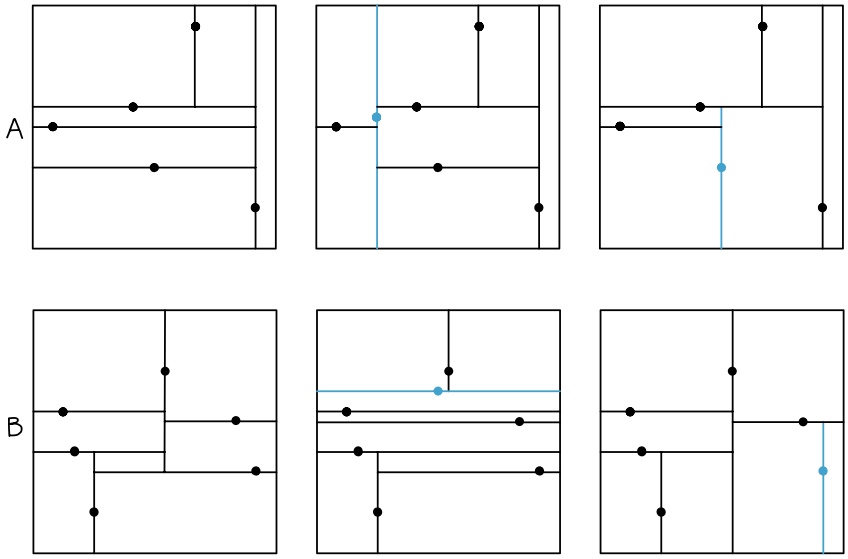

Figure 10: Quadrangulations: A with $k = 5$ and B with $k = 6$ in the first column, an additional point added in the second column and a changed orientation for one point in the third column. The changing vertex is coloured in blue.

11. It is important to realise that the points are only examples and different positions can lead to the same pattern, possibly with different positions and sizes of the rectangles. We can observe that in all but the first case, there are four collisions of lines with the border of the box and two collisions between lines. It is possible to compute exact results for $k = 3$, yet the derivations are very long and tedious and give no further insight into the more general behaviour of this model. Hence, they are not presented here.

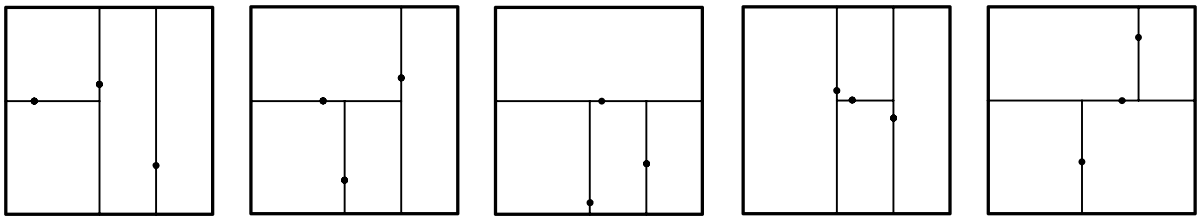

Figure 11: The five different patterns in which the random quadrangulation can result for $k = 3$ points, with some example points included.

Because of the randomness in the number of points, the orientation and the position of the points, combined with the growth of one line depending on the growth of the other lines, analysing the behaviour of this model and deriving distributional results is not a straight forward task. As the entire outcome of this process depends on the length of the lines growing from the vertices, we are interested in deriving probabilistic properties for these. So first, let us define the objects that are necessary for that. Denote the set of points (also called vertices) in Ω from the Poisson process by $\mathcal{V}$. We define the collection

of points $G(0) := \mathcal{V} \subset \Omega$. For $t > 0$, we set

$$G(t) := (\mathcal{L}_v(t), v \in \mathcal{V}), \tag{11}$$

where $\mathcal{L}_v(t)$ is the entire line in both directions that has grown from vertex v up to time t. The graph does not change after time N. Hence, the graph

$$G := (\mathcal{L}_v, v \in \mathcal{V}) := (\mathcal{L}_v(N), v \in \mathcal{V}) \tag{12}$$

is the random quadrangulation obtained from the process.

As the line from any $v \in \mathcal{V}$ grows in two directions, $\mathcal{L}_v$ can be split into two parts for all $v \in \mathcal{V}$ as

$$\mathcal{L}_v = L_v^+ \cup L_v^-, \tag{13}$$

where L_v^+ can be seen as the line upwards for points with vertical orientation and towards the right side for points with horizontal orientation without loss of generality. Correspondingly, L_v^- is the line growing downward for vertical v and toward the left side for horizontal v. Based on this, the following variable can be defined. With a slight abuse of notation, denote L_v the length of the line in the following definition.

Definition 3.1 (Line L_v)**.** *Let $v \in \mathcal{V}$ be a point of the realisation of the Poisson process with assigned orientation. Define L_v to be the length of the line uniformly selected among L_v^+ and L_v^-.*

So whenever the variable L_v is used, it refers to the line once the process has finished. Due to symmetry reasons, exploring distributional characteristics on L_v is representative of L_v^+ and L_v^-. It should be noted that, for a fixed v, one of L_v^+ and L_v^- cannot be larger than $\frac{N}{2}$. Apart from that detail, the growth of these two lines is independent. This will become clear throughout the rest of this section.

Fix $0 \leq t \leq N$ arbitrarily for now. Let us consider the event

$$\{L_v > t\}, \tag{14}$$

which tells that the line L_v has grown further than a distance t, i.e. the line L_v is longer than t at time N. The concepts *time* and *distance* are used interchangeably throughout this work and are often both denoted by t. This is possible because the lines grow at unit speed and depending on the context, either *time* or *distance* is more intuitive to use than the other.

Observe that the area, in which points potentially influence the outcome $\{L_v > t\}$, is diamond shaped with distance t from the centre to the corners. This is illustrated in Figure 12. Denote this area $D_v^{(t)}$, in short D_v when it is clear what t is. Points in the triangle corresponding to the half of the diamond closest to v (shaded grey in Figure 12)

can directly cut off the line L_v. Denote this area $C_v^{(t)}$, short C_v. (Notice that phrases of the type "a point cuts off L_v" should be interpreted as "the line from a point cuts off L_v". Both of these formulations are used throughout this work.)

Definition 3.2 (Cones)**.** *Given a point $v \in \mathcal{V}$ and line L_v, let an area be called a* cone *at v, if it is the area of size t^2 that is enclosed by two diagonals of the same length growing from v in a right angle, and both diagonals are in a 45 degree angle to L_v.*

With this definition, C_v is a cone, specifically the one enclosing L_v. Points in C_v can cut off L_v before it grows a distance t. Because from there, if a point u has orientation orthogonal to L_v, the line from u arrives to the place of collision earlier than L_v (assuming it grows that far). Thus L_v stops growing there, or in other words is cut off (see Figure 12). If a point is outside of the cone C_v, the line arrives to the place of collision later than L_v and thus L_v grows further. Though lines from points in $D_v \setminus C_v$ (the non-shaded area in the figure) do not have direct influence on $\{L_v > t\}$, they can have indirect influence as they can prevent lines in C_v from cutting off L_v. This is also demonstrated in Figure 12. At first, one might think a line from a point u in C_v, which could cut off L_v, can itself be cut off by points outside D_v before reaching L_v. However, that is not the case, as the points cutting off the threatening line from u need to be in a certain close proximity, too, namely in C_u, and regarding the event $\{L_v > t\}$, it holds $C_u \subset D_v$.

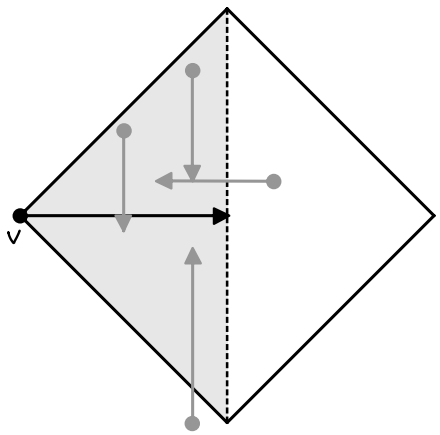

Figure 12: Illustration of the area of influence of a growing line. The shaded area is the *cone* C_v, the entire rotated square is the *diamond* D_v, including examples of other lines growing and influencing L_v.

Whether L_v grows at least a distance t depends on the orientation of a certain group of points within C_v, which we need to define. If a line from a point in C_v grows parallel to L_v, it cannot cut off L_v and is thus no "threat". If it grows orthogonal to L_v, the event $\{L_v > t\}$ can only happen if this line is cut off before reaching L_v. That means, this point, call it u, has to lie in an area where the line from u is blocked by a line parallel to L_v. Figure 13 shows some red and blue lines, where the red lines are cut off by the blue lines growing parallel to L_v – because they lie in a specific area, described next.

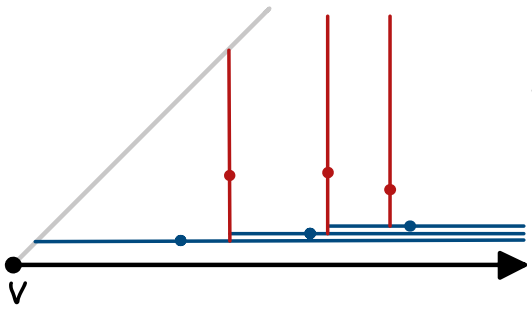

Figure 13: Example of lines parallel to L_v (blue) cutting off all potential threats for L_v (red).

These areas in which points with orientation orthogonal to L_v can lie are also cones, only that they do not enclose the line growing from the points connected to the cones. Figure 14 shows the difference between these different types of cones, where the red area is the C_v on both sides introduced earlier. This is the area in which a point can potentially cut off $\mathcal{L}_v$, an example is given by u_1. However, lines from points in the blue area cannot do that as they arrive to the place of potential collision later than $\mathcal{L}_v$ (if they are orthogonal, an example is depicted by u_2).

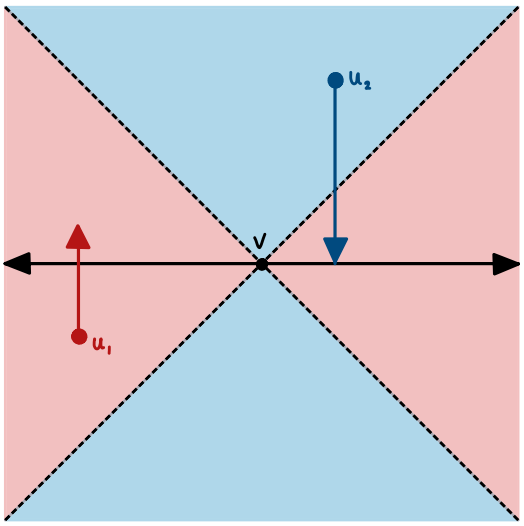

Figure 14: The red areas depict C_v on each side, the blue areas are the "blocked" areas. The line from u_1 cuts off L_v, while the line from u_2 is cut off by L_v.

This means that, if all lines from points in C_v that grow orthogonal to L_v are blocked by points that have lines parallel to L_v, i.e., these points lie in *blocked areas*, then $\{L_v > t\}$ happens. That also means that all points that cannot lie in such blocked areas must grow lines parallel to L_v. This is depicted in Figure 15, where the points that lie in blocked areas are crossed out in red and the points that have to be parallel are depicted with a

line parallel to L_v. The dashed lines mark the borders of the blocked areas. With this in mind, we can define the notion of *tops*.

Definition 3.3 (Tops)**.** *Let $v \in \mathcal{V}$ with a fixed orientation and $u \in \mathcal{V}$ lies in C_v. Let u be called a* top*, if it must be of the same orientation as v in order for $\{L_v > t\}$ to happen.*

A top u must have the same orientation as v in the sense that otherwise, the line from u will definitely cut off L_v.

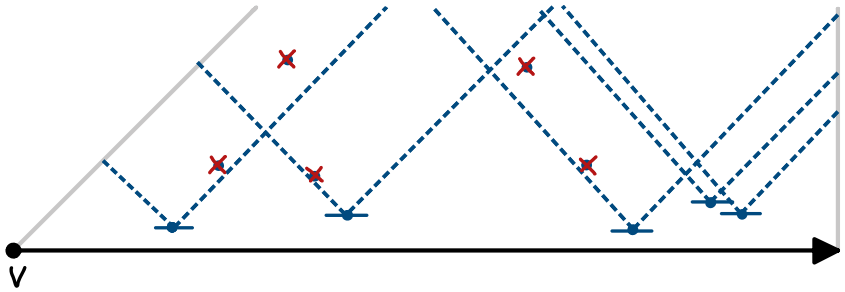

Figure 15: Illustration of *tops*. Points that are crossed out in red are not tops, because they are blocked by lines from other points.

With the notions of cones, blocked areas and tops and an intuition for how the lines influence each other, we are equipped to derive some results on this model.

4 Results

The results are separated into two different parts which correspond to different perspectives on the model. The last part of this section focuses on how these perspectives relate to each other.

4.1 Constant Intensity

For now, $\lambda > 0$ is assumed to be a fixed constant that does not depend on the size of the box N. The theorem that is stated first forms the basis for most of the results presented in this work. It provides an upper bound on the tail probability of the distribution of L_v.

Including all necessary conditions for L_v to grow a certain distance to get an exact probability is highly involved due to the dependence structures. Additionally, the behaviours on both sides of L_v in the cone C_v are not independent, as points in C_v on one side of L_v can influence points in $D_v \setminus C_v$. These can in turn influence points on the other side of L_v in C_v. This is shown in Figure 16, where a line from the left side of L_v cuts off L_v in the left figure, and does not because of an added point on the other side in the right figure. It is not a likely event, but it is possible and must be taken into consideration. Thus, the idea is to obtain a bound by reducing the dependence structure and considering events on subsets of C_v on both sides of L_v that are independent.

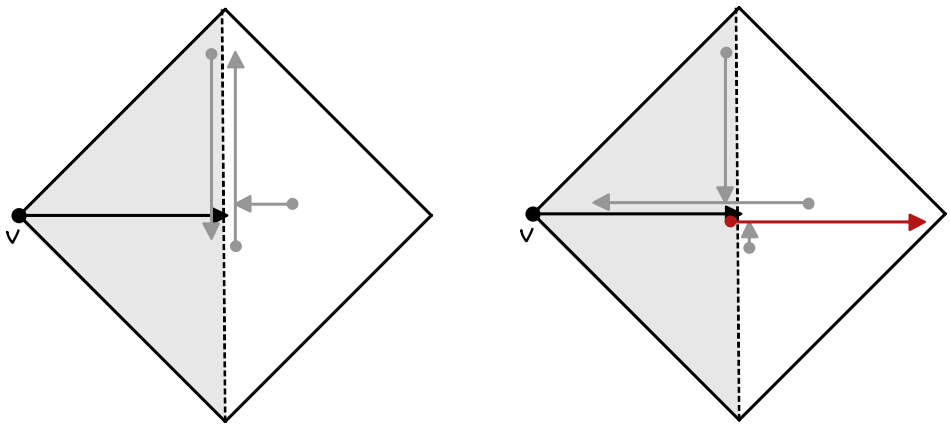

Figure 16: Illustration of the possible interaction between the two sides of L_v without crossing L_v.

Theorem 4.1. *Let $\lambda > 0$ be fixed and select a point $v \in \mathcal{V}$ uniformly. There are constants c and α such that*

$$\mathbb{P}(L_v > t) \leq ce^{-\alpha t} \tag{15}$$

for all N and t.

In particular, if $t > \frac{a}{\sqrt{\lambda}}$ where $a = \frac{8}{(1-e^{-1})(1-\vartheta_{opt})} + 2$ and ϑ_{opt} like in (18), and the distance to both borders parallel to L_v is greater than $\frac{1}{\sqrt{\lambda}}$, then (15) holds for the rate of decay

$$\alpha = \sqrt{\lambda}\vartheta_{opt}^2(1 - \frac{1}{e}) \tag{16}$$

and for the scaling

$$c = \left(\exp\left(\frac{3}{2}(1-\frac{1}{e})\vartheta_{opt}^2\right) + \left(\frac{1}{2}\right)^{-(3+(1-\vartheta_{opt})(1-\frac{1}{e}))}\right)^2, \tag{17}$$

where

$$\vartheta_{opt} = -\frac{\ln(2)}{3} + \sqrt{\frac{\ln(2)^2}{9} + \frac{2\ln(2)}{3}}. \tag{18}$$

Proof. Assume $t > \frac{a}{\sqrt{\lambda}}$ and that the distance from both borders is at least $\frac{1}{\sqrt{\lambda}}$. Consider the area of width $\frac{1}{\sqrt{\lambda}}$ that is adjacent to L_v on an arbitrarily fixed side and is of length t (see area shaded red in Figure 17). Let us also refer to it as *stripe* and denote it by S_v.

We observe that, for the event $\{L_v > t\}$ to happen, it is a necessary condition that the lines from all points in S_v do not cut off L_v. This is necessary for the stripes on both sides. Call the stripe on the other side S'_v. Let us define the following events.

$$B := \{\text{no lines from points in stripe } S_v \text{ cut off } L_v\} \tag{19}$$

$$B' := \{\text{no lines from points in stripe } S'_v \text{ cut off } L_v\} \tag{20}$$

$$\bar{B} := \{\text{no lines from points in } C_v \setminus (S_v \cup S'_v) \text{ cut off } L_v\} \tag{21}$$

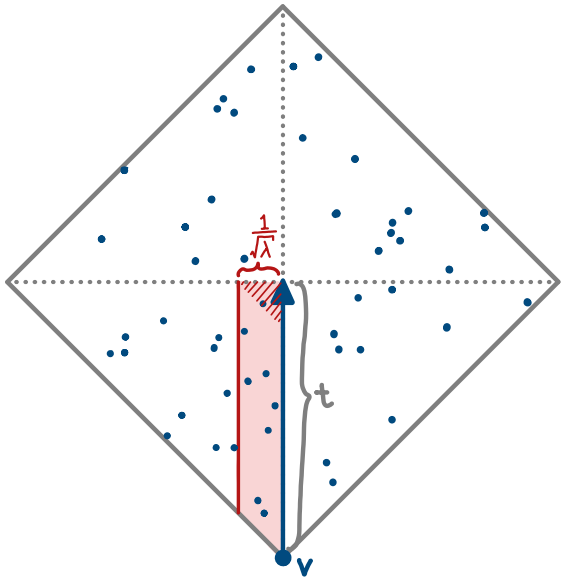

Figure 17: Illustration of the stripe S_v of width $\frac{1}{\sqrt{\lambda}}$ and length t, shaded in red.

Then,

$$B \cap B' \cap \bar{B} = \{L_v > t\} \tag{22}$$

and thus

$$\{L_v > t\} \subset B \cap B', \tag{23}$$

which implies

$$\mathbb{P}(L_v > t) \leq \mathbb{P}(B \cap B'). \tag{24}$$

However, the events B and B' are not independent. This is because lines from points in a triangle in the square in the stripe S_v furthest away from v, the striped area in Figure 17, can indirectly influence what happens in the corresponding area in the other stripe S'_v, in the way that was also illustrated in Figure 16. We keep this in mind for now.

We recall the definition of tops (see Definition 3.3) and note that, in order for L_v to grow longer than a distance t, all points that are tops in S_v and S'_v need to have the same orientation as v. Thus, the question is how many tops there are. For that, divide the stripes into boxes with side length $\frac{1}{\sqrt{\lambda}}$, starting from the end of the stripe with v, as illustrated in Figure 18. This leaves a triangle at v and possibly a fraction of a square at the other end of the stripe.

In order to only be left with boxes (squares) that have the same distribution of the number of points in them, we cut away the triangle and the possibly left over partial square, as they have different areas and therefore different Poisson distributions. Additionally, we cut away one more box furthest away from v to ensure that we obtain non-interfering areas on both sides of L_v. We denote this adjusted stripe by $\tilde{S}_v$, and

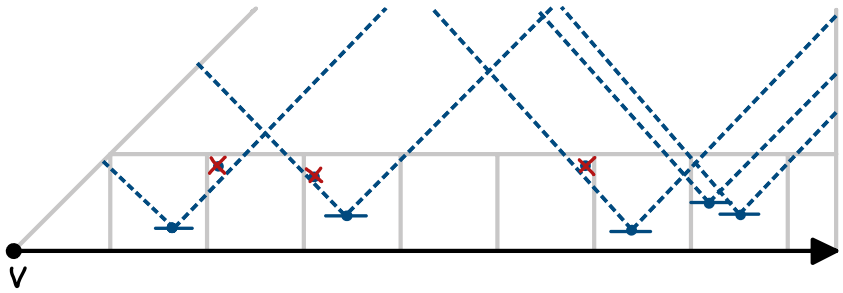

Figure 18: Illustration of tops. Points that are crossed out in red are not tops, because they are blocked by lines of other points. The boxes which the stripe S_v is divided in are also shown.

correspondingly the one on the other side by $\tilde{S}'_v$. We also define the adjusted events:

$$\tilde{B} := \{\text{no lines from points in the adjusted stripe } \tilde{S}_v \text{ cut off } L_v\}, \tag{25}$$

$$\tilde{B}' := \{\text{no lines from points in the adjusted stripe } \tilde{S}'_v \text{ cut off } L_v\}, \tag{26}$$

which are now independent and have the same probability due to symmetry. Furthermore it holds that $\tilde{B} \cap \tilde{B}' \supset B \cap B'$. Combining that, we obtain

$$\mathbb{P}(L_v > t) \leq \mathbb{P}(B \cap B') \leq \mathbb{P}(\tilde{B} \cap \tilde{B}') = \mathbb{P}(\tilde{B}) \cdot \mathbb{P}(\tilde{B}') = \left(\mathbb{P}(\tilde{B})\right)^2. \tag{27}$$

Let w denote the number of boxes in $\tilde{S}_v$ that contain at least one point and regard this as fixed for now, i.e., as one realisation, which is $w = 8$ in figure 19. Then there are at least $\lfloor \frac{w}{3} \rfloor - 2$ tops because of the following arguments. The points in some boxes might be in areas blocked by lines from other points and are therefore not tops. Lines from points in one box can only block parts of their neighbouring boxes, not further away. This is because of the squared shape of the boxes. We can refer back to Figures 18 and 19 to see that, where points which are not tops are crossed out in red. Moreover, the points in the boxes furthest to the right and to the left can be in areas blocked by lines from points outside of $\tilde{S}_v$. Figure 19 shows an extreme case, where there are $w = 8$ boxes that contain points but only two tops. Having only $\lfloor \frac{w}{3} \rfloor - 2$ tops is unlikely, because it is unlikely that the points in three consecutive boxes are always in that type of position. It is also likely that there are boxes that contain more than one point and more than one top. In that sense, Figure 18 shows a more typical number of filled boxes in relation to tops than Figure 19 does.

Now, we can get to the technical details of this approach. Because of (27), it is enough to derive a bound for one side. Define

$$M := \#\{\text{tops in } \tilde{S}_v\}, \tag{28}$$

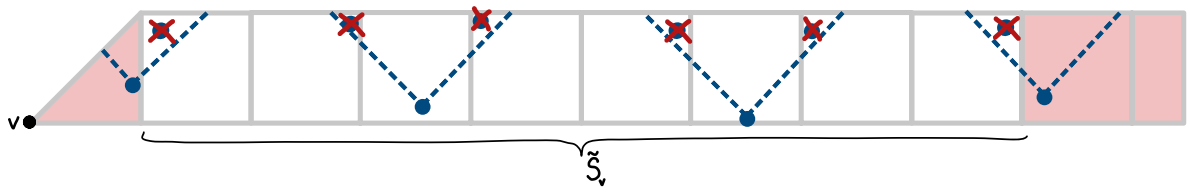

Figure 19: Illustration of S_v and $\tilde{S}_v$ with the minimum possible number of tops given the $w = 8$ filled boxes in $\tilde{S}_v$. The area shaded in red are the boxes in $S_v \setminus \tilde{S}_v$

for which the distribution is unknown. By its definition, $\tilde{S}_v$ is made of

$$b_t := \lfloor t \cdot \sqrt{\lambda} \rfloor - 2 \geq t \cdot \sqrt{\lambda} - 3 \tag{29}$$

squares, each with area $\frac{1}{\lambda}$. Thus, for the number of points K_i in box $i, i \in \{1, \ldots, b_t\}$, it holds that

$$K_i := \#\{\text{points in box } i\} \sim \text{Poi}(1). \tag{30}$$

It follows that a box contains at least one point with probability $(1 - \frac{1}{e})$, which is characterised by the Bernoulli variable $\xi_i \sim \text{Bin}(1, 1 - \frac{1}{e})$, $i \in \{1, \ldots, b_t\}$. These variables are all independent because of the independent increments of a Poisson process. So denote the random variable ξ as the number of filled boxes in $\tilde{S}_v$, which then has a Binomial distribution

$$\xi := \sum_{i=1}^{b_t} \xi_i \sim \text{Bin}\left(b_t, 1 - \frac{1}{e}\right) \tag{31}$$

with expected value $\mu = (1 - \frac{1}{e})b_t$ and of which the earlier w can be seen as a realisation. Due to the explained relationship between the number of tops and filled boxes, $M \geq \lfloor \frac{\xi}{3} \rfloor - 2$, from which it follows that $3M + 8 \geq \xi$. This implies that M is stochastically dominant over $\lfloor \frac{\xi}{3} \rfloor - 2$ and thus

$$\mathbb{P}(M \leq m) \leq \mathbb{P}(\lfloor \xi/3 \rfloor - 2 \leq m). \tag{32}$$

The event $\tilde{B}$ (see (25)) means that all tops need to have orientation parallel to L_v, which has probability $\frac{1}{2}$ for each top independently, so $\mathbb{P}(\tilde{B}|M = m) = \left(\frac{1}{2}\right)^m$. Let $\vartheta \in (0, 1)$, which is needed for a Chernoff bound, be chosen as

$$\vartheta := \vartheta_{\text{opt}} := -\frac{\ln(2)}{3} + \sqrt{\frac{\ln(2)^2}{9} + \frac{2\ln(2)}{3}}. \tag{33}$$

This is optimal in a sense explained at a later point. Define γ such that it is the largest non-negative integer for which it holds that $3\gamma + 8 \leq (1 - \vartheta)\mu$. This is also the reason for the assumption $t > \frac{a}{\sqrt{\lambda}}$, as $(1 - \vartheta)\mu$ must be at least 8 for the chosen (positive) ϑ. Using the law of total probability in (34), the stochastic dominance of M in (39) and

the Chernoff bound for the lower tail of a Binomial distribution in (41), we obtain the following bound.

$$\mathbb{P}(\tilde{B}) = \sum_{m=0}^{\infty} \mathbb{P}(\tilde{B}|M=m)\,\mathbb{P}(M=m) \tag{34}$$

$$= \sum_{m=0}^{\gamma} \mathbb{P}(\tilde{B}|M=m)\,\mathbb{P}(M=m) + \sum_{m=\gamma+1}^{\infty} \mathbb{P}(\tilde{B}|M=m)\,\mathbb{P}(M=m) \tag{35}$$

$$\leq \sum_{m=0}^{\gamma} \mathbb{P}(M=m) + \sum_{m=\gamma+1}^{\infty} \mathbb{P}(\tilde{B}|M=m) \tag{36}$$

$$= \mathbb{P}(M \leq \gamma) + \sum_{m=\gamma+1}^{\infty} \left(\frac{1}{2}\right)^m \tag{37}$$

$$= \mathbb{P}(M \leq \gamma) + \left(\frac{1}{2}\right)^{\gamma} \tag{38}$$

$$\leq \mathbb{P}(\xi \leq 3\gamma + 8) + \left(\frac{1}{2}\right)^{\gamma} \tag{39}$$

$$\leq \mathbb{P}(\xi \leq (1-\vartheta)\mu) + \left(\frac{1}{2}\right)^{\frac{1}{3}(1-\vartheta)\mu - 3} \tag{40}$$

$$\leq \exp\left(-\frac{1}{2}\vartheta^2\mu\right) + \left(\frac{1}{2}\right)^{\frac{1}{3}(1-\vartheta)\mu - 3} \tag{41}$$

$$\leq \exp\left(-\frac{1}{2}\vartheta^2(1-\frac{1}{e})(t\cdot\sqrt{\lambda}-3)\right) + \exp\left(-\frac{\ln(2)}{3}(1-\vartheta)(1-\frac{1}{e})(t\cdot\sqrt{\lambda}-3) + 3\ln(2)\right) \tag{42}$$

Since the Chernoff bound holds for any $\vartheta \in (0,1)$, it can be chosen such that it is optimal for this case. Here it is optimal when the rate of decay, i.e., the factor before t in the exponential terms, is the same in both parts of the sum, as that maximises the overall rate of decay and hence gives the strongest bound. This is achieved when

$$\frac{1}{2}\vartheta^2 = \frac{\ln(2)}{3}(1-\vartheta), \tag{43}$$

which is the reason for the optimal value presented in (18). Simplifying (42) with this yields

$$\mathbb{P}(\tilde{B}) \leq \underbrace{\left(\exp\left(\frac{3}{2}(1-\frac{1}{e})\vartheta_{\text{opt}}^2\right) + \left(\frac{1}{2}\right)^{-(3+(1-\vartheta_{\text{opt}})(1-\frac{1}{e}))}\right)}_{=:\tilde{c}} \cdot \exp\left(-\underbrace{\frac{\sqrt{\lambda}\vartheta_{\text{opt}}^2}{2}(1-\frac{1}{e})}_{=:\tilde{\alpha}}\, t\right) \tag{44}$$

Then (27) implies that $c = \tilde{c}^2$ and $\alpha = 2\tilde{\alpha}$.

When the distance to one of the borders parallel to L_v is less than $\frac{1}{\sqrt{\lambda}}$, the stripe on that side does not fully lie in Ω and the upper bound does not hold for c and α as before. However, the exponential upper bound is still obtained for the constants $\tilde{c}$ and $\tilde{\alpha}$, because for large enough N, the distance is always at least $\frac{1}{\sqrt{\lambda}}$ to one of the parallel borders.

□

Remark 4.1. *The distance to the border in the direction of L_v does not affect that the values presented for c and α hold in the upper bound. This is because L_v is guaranteed to be cut off by the border in case the distance is less than t, making the probability for $\{L_v > t\}$ even smaller, in fact it is 0 in that case. Hence the upper bound is still correct.*

Theorem 4.2. *Let $\lambda > 0$ be fixed and select a point $v \in \mathcal{V}$ uniformly. There are constants c and α such that, for all t and N,*

$$\mathbb{P}(L_v > t) \geq ce^{-\alpha t}. \tag{45}$$

In particular, if the distance to the border in the direction of L_v is at least t and $t > \frac{2}{\sqrt{\lambda}}$, then (45) holds for $c = \frac{1}{16}$ and $\alpha = 2\ln\left(\frac{8e}{e-1}\right)\sqrt{\lambda}$.

Remark 4.2. *For the particular values of c and α, we require the distance from the border in the direction of L_v to be at least t, because if it is not, the probability for $\{L_v > t\}$ is 0 as it is definitely stopped by the border. Then the lower bound does not hold for the presented values, and it is not needed.*

Before going into the technical details of the proof, the idea behind it needs to be explained. From the upper bound in Theorem 4.1, we recall the observation that all tops (illustrated in Figure 15) need to have lines growing parallel to L_v. This is a necessary condition for $\{L_v > t\}$ to happen and makes it possible to obtain an upper bound. A sufficient condition is needed to obtain a lower bound. This can be a condition which requires more points than necessary to be parallel to L_v, so when conditioning on that, the event $\{L_v > t\}$ is guaranteed to happen. The question is, how to define that group of points that is required to have the same orientation as v, or in other words, in what area are points required to grow lines parallel to L_v?

Figure 20 shows an example of the stripe S_v again as it was defined in the proof of Theorem 4.1, so adjacent to L_v and of width $\frac{1}{\sqrt{\lambda}}$. It is split into boxes and can contain some points, specifically tops. Let us imagine that we know the number of points in the stripe, but not outside of it, so there might be points outside of the stripe which are not depicted in the figure. The shaded areas above the points in the stripes indicate the areas from which no points can grow lines that cut off L_v. This is because they will be blocked by the lines from the tops before reaching L_v, if not already before. These are the *blocked areas*. So conditioned that all points outside of the area blocked by lines from tops grow parallel to L_v (shaded in the figure), the line L_v grows at least a distance t

(when assuming this for both sides). Hence, this is a sufficient condition. The question is how to bound this area, since the exact value of it depends entirely on the number, orientation and position of points, and is therefore quite involved.

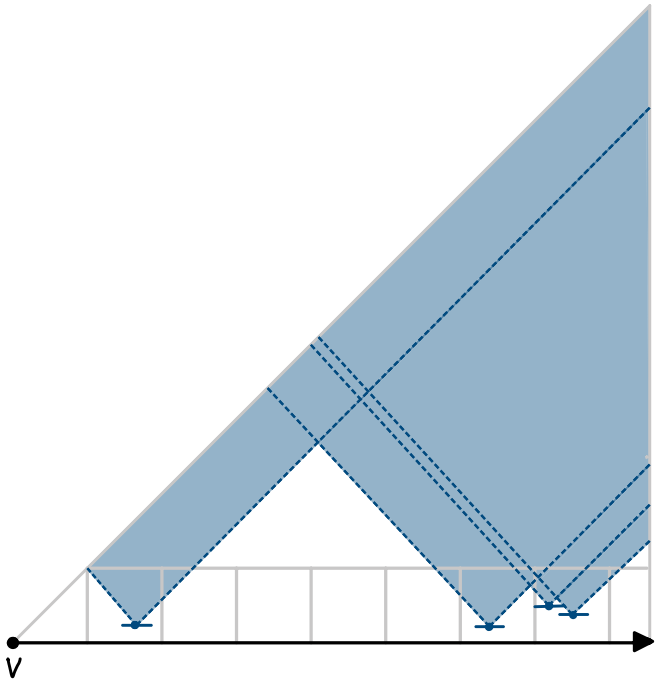

Figure 20: Illustration of the area where the orientation of points does not affect $\{L_v > t\}$, shaded in blue. I.e., the area blocked by lines from tops. The line L_v is of length t.

It is possible to employ the number of empty and filled boxes again, this time focusing on the number of empty boxes. For now, assume that there is a fixed number w of empty boxes in the stripe S_v, as illustrated for $w = 6$ on the left side in Figure 21. The area in which lines from points are not blocked by lines from tops (i.e., the non-shaded area) is the largest when the empty boxes are consecutive and as far away from v as possible, as shown in the figure. Considering the right illustration in the figure, where there is a point in the box furthest away from v, observe that the area not shaded in blue (i.e., the area from which lines might cut off L_v) is immensely smaller than before. This can give a better bound because then, less points need to be required to be parallel to L_v.

That area is still largest when the empty boxes lie consecutively furthest away from v. When the box furthest away from v contains any points, the distance a point in the non-blocked area can have from L_v is no larger than $\frac{1}{\sqrt{\lambda}}(2 + \frac{w}{2})$ in any case. Due to the use of a probability generating function at some later point in the proof, it is desirable to have an area that does not contain a squared term of the number of empty boxes w. Because of that, we consider the entire area shaded green in Figure 21, even if it includes an area outside of C_v. Note that the size of this shaded area depends on the number of empty boxes w.

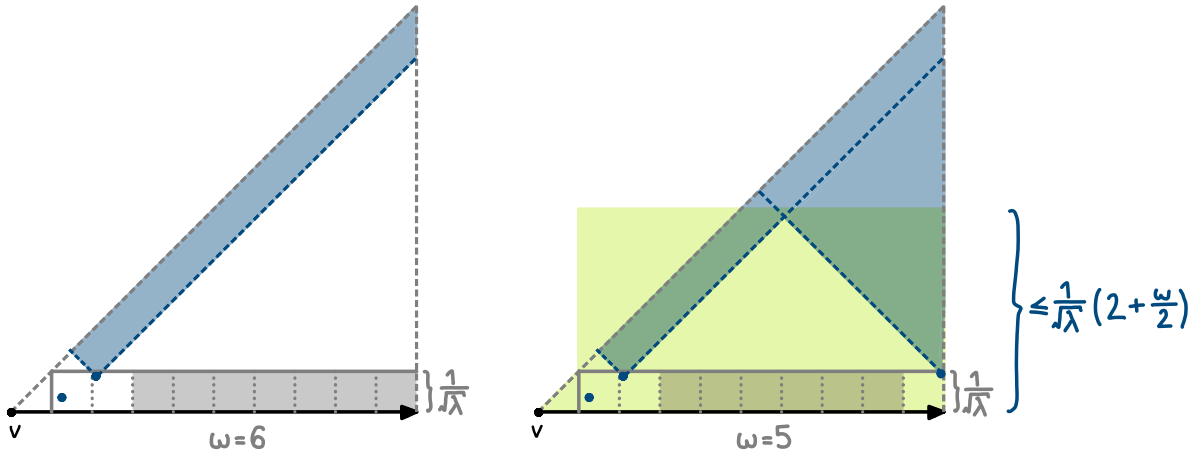

Figure 21: Illustration of possible scenario when not conditioning on a point in the last box with $w = 6$ (left) and of S_v^w, shaded in light green, with the example of $w = 5$ empty boxes in the worst possible location (right).

Before we formalise the idea of the proof, we state the following useful observations.

Proposition 4.1. *Let $K \sim Poi(1)$ and $K^{Tr} \sim PoiTr(1)$. Then $K + 1$ has stochastic dominance over K^{Tr}, i.e., $\mathbb{P}(K + 1 \leq k) \leq \mathbb{P}(K^{Tr} \leq k), k \in \mathbb{N}$.*

Proof. The cumulative distribution functions are the following (recall (4) and (6)):

$$\mathbb{P}(K + 1 \leq k) = \mathbb{P}(K \leq k - 1) = \sum_{j=0}^{k-1} \frac{1}{e \cdot j!} = \frac{1}{e}\left(\sum_{j=0}^{k} \frac{1}{j!} - \frac{1}{k!}\right), \tag{46}$$

$$\mathbb{P}(K^{Tr} \leq k) = \frac{\sum_{j=0}^{k} \frac{1}{j!} - 1}{e - 1} = \frac{1}{e - 1}\left(\sum_{j=0}^{k} \frac{1}{j!} - 1\right). \tag{47}$$

Furthermore, it holds that

$$\mathbb{P}(K + 1 \leq k) \leq \mathbb{P}(K^{Tr} \leq k) \tag{48}$$

because plugging in (46) and (47) yields the equivalent inequality

$$\sum_{j=0}^{k} \frac{1}{j!} \geq e - \frac{e - 1}{k!}, \tag{49}$$

which holds for all $k \in \mathbb{N}$. Let us prove this last statement.

It can be calculated that it holds for $k = 1, 2, 3$. Next, inspect the increase for the left- and right-hand side from k to $k + 1$. For the left-hand side, this is

$$\sum_{j=0}^{k+1} \frac{1}{j!} - \sum_{j=0}^{k} \frac{1}{j!} = \frac{1}{k + 1} \tag{50}$$

and for the right-hand side, it is

$$e - \frac{e-1}{(k+1)!} - \left(e - \frac{e-1}{k!}\right) = \frac{e-1}{k!}\left(1 - \frac{1}{k+1}\right). \tag{51}$$

Relating (50) and (51),

$$\frac{1}{k+1} \geq \frac{e-1}{k!}\left(1 - \frac{1}{k+1}\right) \tag{52}$$

is equivalent to

$$(k-1)! \geq e - 1, \tag{53}$$

which holds for all $k \geq 3$. So since (49) holds for $k = 1, 2, 3$ and the increase for the left-hand side is larger than for the right-hand side for all $k \geq 3$, the inequality must hold for all $k \in \mathbb{N}$, concluding the proof. □

Corollary 4.1. *Let $K_1, \ldots, K_n \sim Poi(1)$, $K \sim Poi(\lambda)$, $K_1^{Tr}, \ldots, K_n^{Tr} \sim PoiTr(1)$ and $K' \sim Poi(\lambda + n)$ all independent. Then for all $k \geq n$:*

$$\mathbb{P}(K' \leq k - n) \leq \mathbb{P}(K + K_1^{Tr} + \ldots + K_n^{Tr} \leq k).$$

Proof. Observe that $K + K_1 + \cdots + K_n \overset{d}{=} K'$. Each $K_i + 1$ has stochastic dominance over $K_i^{Tr}, i \in \{1, \ldots, n\}$. This together gives:

$$\begin{aligned}
&\mathbb{P}(K + K_1^{Tr} + \ldots + K_n^{Tr} \leq k) \\
&\quad \geq \mathbb{P}(K + (K_1 + 1) + \ldots + (K_n + 1) \leq k) \\
&\quad = \mathbb{P}(K + K_1 + \ldots + K_n \leq k - n) \\
&\quad = \mathbb{P}(K' \leq k - n).
\end{aligned}$$

□

Proof of Theorem 4.2. First, let us determine the number of boxes in the stripe S_v of width $\frac{1}{\sqrt{\lambda}}$. Instead of cutting off the potential fraction of a box furthest away from v we increase it to a whole box as we are obtaining a lower bound in this case. Furthermore, we cut away the triangle at v, leaving

$$b_t := \lceil t \cdot \sqrt{\lambda} \rceil - 1 \tag{54}$$

boxes. Formalising the idea of the area shaded green in Figure 21, we denote this area by S_v^w, as it depends on the number of empty boxes w. It is a rectangle with a height of $\frac{1}{\sqrt{\lambda}}(2 + \frac{w}{2})$ and a width of $b_t \cdot \frac{1}{\sqrt{\lambda}} \leq t$, plus the attached triangle of area $\frac{1}{2\lambda}$ as depicted by

the region shaded green in Figure 21. It is of size

$$A(S_v^w) := \frac{1}{\sqrt{\lambda}}(2+\frac{w}{2})\cdot(b_t\cdot\frac{1}{\sqrt{\lambda}})+\frac{1}{2\lambda} \leq \frac{1}{\sqrt{\lambda}}(2+\frac{w}{2})t+\frac{1}{2\lambda} =: A. \tag{55}$$

We define the following events:

$$B := \{L_v \text{ is not cut off from points in } C_v \text{ on the side of } S_v\}, \tag{56}$$

$$B_w := \{\text{all points in } S_v^w \text{ have the same orientation as } v\}. \tag{57}$$

As explained with the illustrations in Figure 21, we want to condition on that the box furthest away from v (call it *last box*) contains points separately. Let ζ denote the (random) number of empty boxes within the other $b_t - 1$ boxes in S_v. Then

$$\zeta \sim \text{Bin}\left(b_t - 1, \frac{1}{e}\right). \tag{58}$$

Let us define

$$\nu := \mathbb{1}(\text{last box in } S_v \text{ non-empty}) \sim \text{Bin}\left(1, 1-\frac{1}{e}\right). \tag{59}$$

All the definitions so far considered only the events on one side of L_v, but of course L_v only grows longer than a distance t if it is not cut off from either of the sides. So with w' empty boxes in the stripe S'_v on the other side, let ${S'}_v^w$ denote our area of consideration (shaded green in Figure 21) on the other side. We also define

$$B' := \{L_v \text{ is not cut off from points in } C_v \text{ on the side of } S'_v\}, \tag{60}$$

$$B'_w := \{\text{all points in } {S'}_v^w \text{ have the same orientation as } v\}, \tag{61}$$

$$\nu' := \mathbb{1}(\text{last box in } S'_v \text{ non-empty}) \sim \text{Bin}\left(1, 1-\frac{1}{e}\right), \tag{62}$$

$$\zeta' \sim \text{Bin}\left(b_t - 1, \frac{1}{e}\right) \tag{63}$$

as the corresponding events and random variables on the other side. Note that

$$\{L_v > t\} = B \cap B'. \tag{64}$$

Since B and B' are not independent by the arguments at the beginning of the section and illustrated in Figure 16, let us show that we can use our bounds independently. For that, observe that

$$B \cap B' \supseteq B_w \cap B'_w. \tag{65}$$

Furthermore, ζ, ζ', ν and ν' are independent due to the independent increments of the Poisson process. The orientation of points is independent of the number of points. Finally,

B_w is independent of the number of points and empty boxes on the other side (ζ' and ν') and vice versa. With these arguments, the following holds:

$$\begin{aligned}
\mathbb{P}(B \cap B') &= \sum_{i=0}^{1}\sum_{j=0}^{1}\sum_{w=0}^{b_t-1}\sum_{w'=0}^{b_t-1} \mathbb{P}(B \cap B'|\zeta = w, \zeta' = w', \nu = i, \nu' = j)\, \mathbb{P}(\zeta = w|\zeta' = w', \nu = i, \nu' = j) \\
&\qquad \cdot \mathbb{P}(\zeta' = w'|, \nu = i, \nu' = j)\, \mathbb{P}(\nu = i|\nu' = j)\, \mathbb{P}(\nu' = j) \\
&\geq \sum_{i=0}^{1}\sum_{j=0}^{1}\sum_{w=0}^{b_t-1}\sum_{w'=0}^{b_t-1} \mathbb{P}(B_w \cap B'_w|\zeta = w, \zeta' = w', \nu = i, \nu' = j)\mathbb{P}(\zeta = w)\, \mathbb{P}(\zeta' = w')\, \mathbb{P}(\nu = i)\, \mathbb{P}(\nu' = j) \\
&= \sum_{i=0}^{1}\sum_{j=0}^{1}\sum_{w=0}^{b_t-1}\sum_{w'=0}^{b_t-1} \mathbb{P}(B_w|\zeta = w, \nu = i)\, \mathbb{P}(B'_w|\zeta' = w', \nu' = j)\, \mathbb{P}(\zeta = w)\, \mathbb{P}(\zeta' = w')\, \mathbb{P}(\nu = i)\, \mathbb{P}(\nu' = j) \\
&= \sum_{i=0}^{1}\sum_{w=0}^{b_t-1} \mathbb{P}(B_w|\zeta = w, \nu = i)\, \mathbb{P}(\zeta = w)\, \mathbb{P}(\nu = i) \\
&\quad \cdot \sum_{j=0}^{1}\sum_{w'=0}^{b_t-1} \mathbb{P}(B'_w|\zeta' = w', \nu' = j)\, \mathbb{P}(\zeta' = w')\, \mathbb{P}(\nu' = j). \qquad (66)
\end{aligned}$$

Define

$$K_w := \#\{\text{points in } S_v^w\} \sim \text{Poi}(\lambda A(S_v^w)) \qquad (67)$$

and denote $\tilde{K}_w$ the number of points in the area S_v^w without the w empty boxes. The latter set has a total area $\frac{w}{\lambda}$. Hence,

$$\tilde{K}_w \sim \text{Poi}\left(\lambda \cdot \left(A(S_v^w) - \frac{w}{\lambda}\right)\right). \qquad (68)$$

Furthermore, denote $\tilde{\lambda} = \lambda \cdot (A(S_v^w) - \frac{w}{\lambda})$, where $A(S_v^w)$ is as defined in (55), so $\tilde{K}_w \sim \text{Poi}(\tilde{\lambda})$. Note that $\tilde{\lambda} \leq \lambda A$ (because of (55)). Denote $U_1, \ldots, U_{b_t} \sim \text{Poi}(1)$ as the i.i.d. Poisson distributed points in each of the b_t boxes in S_v and $U_1^{Tr}, \ldots, U_{b_t}^{Tr} \sim \text{PoiTr}(1)$ the zero-truncated version of these variables. Let

$$\bar{K}_w := \#\{\text{points in } S_v^w \setminus S_v\}. \qquad (69)$$

Then $K_w = \bar{K}_w + U_1 + \cdots + U_{b_t}$ and $\tilde{K}_w \overset{d}{=} \bar{K}_w + U_{w+1} + \ldots + U_{b_t}$ conditioned that $U_i = 0$ for all $1 \leq i \leq w$.

Equipped with this, we begin by reducing the bound to the case when $\nu = 1$, i.e., the last box is filled:

$$\begin{aligned}
&\sum_{i=0}^{1}\sum_{w=0}^{b_t-1} \mathbb{P}(B_w|\zeta = w, \nu = i)\, \mathbb{P}(\zeta = w)\mathbb{P}(\nu = i) \qquad (70) \\
&\qquad \geq (1 - \frac{1}{e}) \sum_{w=0}^{b_t-1} \mathbb{P}(B_w|\zeta = w, \nu = 1)\, \mathbb{P}(\zeta = w). \qquad (71)
\end{aligned}$$

We save the factor $(1-\frac{1}{e})$ for the rest of the computations and continue with the law of probability and the independence of ν, ζ and the orientation of points. Recall the definition of B_w (see (57)) and that each point has orientation like v with probability $\frac{1}{2}$.

$$\sum_{w=0}^{b_t-1}\mathbb{P}(B_w|\zeta=w,\nu=1)\,\mathbb{P}(\zeta=w) \tag{72}$$

$$=\sum_{w=0}^{b_t-1}\sum_{k=0}^{\infty}\mathbb{P}(B_w|K_w=k,\zeta=w,\nu=1)\,\mathbb{P}(K_w=k|\zeta=w,\nu=1)\;\mathbb{P}(\zeta=w) \tag{73}$$

$$=\sum_{w=0}^{b_t-1}\mathbb{P}(\zeta=w)\sum_{k=0}^{\infty}\left(\frac{1}{2}\right)^k\mathbb{P}(K_w=k|\zeta=w,\nu=1) \tag{74}$$

Let $\tilde{k}=\tilde{\lambda}+b_t-w$, chosen so that the following fact can be used in (80). For some $\mu>0$ and some $Z\sim\mathrm{Poi}(\mu)$, it holds that $\mathbb{P}(Z\leq\mu)>\frac{1}{2}$ [14]. We recall that $\lambda A=\sqrt{\lambda}(2+\frac{w}{2})t+\frac{1}{2}$.

$$\sum_{w=0}^{b_t-1}\mathbb{P}(\zeta=w)\sum_{k=0}^{\infty}\left(\frac{1}{2}\right)^k\mathbb{P}(K_w=k|\zeta=w,\nu=1) \tag{75}$$

$$\geq\sum_{w=0}^{b_t-1}\left(\frac{1}{2}\right)^{\tilde{k}}\mathbb{P}(K_w\leq\tilde{k}|\zeta=w,\nu=1)\mathbb{P}(\zeta=w) \tag{76}$$

$$=\sum_{w=0}^{b_t-1}\left(\frac{1}{2}\right)^{\tilde{k}}\mathbb{P}(\bar{K}_w+U_1+\cdots+U_w+U_{w+1}+\cdots+U_{b_t}\leq\tilde{k}|\zeta=w,\nu=1)\mathbb{P}(\zeta=w) \tag{77}$$

$$=\sum_{w=0}^{b_t-1}\left(\frac{1}{2}\right)^{\tilde{k}}\mathbb{P}(\bar{K}_w+U_{w+1}^{Tr}+\cdots+U_{b_t}^{Tr}\leq\tilde{k})\mathbb{P}(\zeta=w) \tag{78}$$

$$\overset{Cor.4.1}{\geq}\sum_{w=0}^{b_t-1}\left(\frac{1}{2}\right)^{\tilde{k}}\mathbb{P}(\tilde{K}_w\leq\tilde{k}-b_t+w)\,\mathbb{P}(\zeta=w) \tag{79}$$

$$>\sum_{w=0}^{b_t-1}\left(\frac{1}{2}\right)^{\tilde{\lambda}+b_t-w+1}\mathbb{P}(\zeta=w) \tag{80}$$

$$\overset{\tilde{\lambda}\leq\lambda A}{\geq}\sum_{w=0}^{b_t-1}\left(\frac{1}{2}\right)^{\lambda A+b_t-w+1}\binom{b_t-1}{w}\left(\frac{1}{e}\right)^w\left(1-\frac{1}{e}\right)^{b_t-1-w} \tag{81}$$

$$\geq\frac{1}{4}\left(\frac{1}{8}\right)^{\sqrt{\lambda}t}\sum_{w=0}^{b_t-1}\left(\left(\frac{1}{2}\right)^{\frac{\sqrt{\lambda}t}{2}-1}\right)^w\binom{b_t-1}{w}\left(\frac{1}{e}\right)^w\left(1-\frac{1}{e}\right)^{b_t-1-w} \tag{82}$$

We can now use the probability generating function for Binomial random variables (see (9)).

$$\frac{1}{4}\left(\frac{1}{8}\right)^{\sqrt{\lambda}t}\sum_{w=0}^{b_t-1}\left(\left(\frac{1}{2}\right)^{\frac{\sqrt{\lambda}t}{2}-1}\right)^{w}\binom{b_t-1}{w}\left(\frac{1}{e}\right)^{w}\left(1-\frac{1}{e}\right)^{b_t-1-w} \tag{83}$$

$$=\frac{1}{4}\left(\frac{1}{8}\right)^{\sqrt{\lambda}t}\left(1-\frac{1}{e}+\frac{1}{e}\left(\frac{1}{2}\right)^{\frac{\sqrt{\lambda}t}{2}-1}\right)^{b_t-1} \tag{84}$$

$$\geq\frac{1}{4}\left(\frac{1}{8}\right)^{\sqrt{\lambda}t}\left(1-\frac{1}{e}\right)^{\sqrt{\lambda}t-1} \tag{85}$$

Putting back in the factor $(1-\frac{1}{e})$ from (71), the final bound is

$$\sum_{w=0}^{b_t-1}\mathbb{P}(\zeta=w)\sum_{k=0}^{\infty}\left(\frac{1}{2}\right)^{k}\mathbb{P}(K_w=k|\zeta=w,\nu=1)\geq\frac{1}{4}\exp\left(-\ln\left(\frac{8e}{e-1}\right)\sqrt{\lambda}t\right). \tag{86}$$

Due to (66), squaring this expression yields a lower bound for $\mathbb{P}(L_v>t)$ with the constants c and α as stated above in the theorem. □

We will now consider a different characteristic that describes the behaviour of this model and we start by defining it.

Definition 4.1 (Escaping lines)**.** *Consider a realisation of the quadrangulation at time N, i.e., all lines have stopped growing. Call the lines that reach the border of Ω* escaping lines.

Note that here, the word *line* is used in the sense that each vertex has two lines. The expected value of the number of escaping lines is bounded from above in the following theorem.

Theorem 4.3. *Let Y be the number of escaping lines and assume a $Poi(\lambda N^2), \lambda>0$, process on Ω. Then, for all $\beta>0$, there exists a constant $C(\beta)$ such that, for large N,*

$$\mathbb{E}(Y)\leq C(\beta)N^{1+\beta}. \tag{87}$$

Asymptotically in N, this bound can be made arbitrarily close to linear in N. The proof of this theorem has the following key ideas. First, observe that if there was a fixed number of points in Ω, say k, and $\mathbb{E}(Y_v)$ denotes the expected value of the indicator that L_v reaches the border (v uniformly selected from $\mathcal{V}$), it would hold that $\mathbb{E}(Y)=2k\mathbb{E}(Y_v)$, as each point grows a line in two opposite directions. However in this case, the number of points K is random and thus we have a random sum of expected values where the expected value $\mathbb{E}(Y_v)$ depends on K. So Wald's identity cannot be used. Because of this, Theorem 4.1 needs to be slightly adjusted in order to use it.

Furthermore, the law of total expectation is essential as well as the independent increments of a Poisson process. Finally, the law of total probability in the continuous case can be utilised to find an upper bound for $\mathbb{E}(Y_v)$ together with the adjusted version of Theorem 4.1. Consider the following Lemma first.

Lemma 4.1. *Let $K \sim Poi(\lambda N^2)$ and $\beta > 0$ be fixed. There exist constants c and α such that, for all t and N,*

$$\mathbb{P}(L_v > t | K \leq \lambda N^{2+\beta}) \leq C_1 c e^{-\alpha t}. \tag{88}$$

In particular, if $t > \frac{a}{\sqrt{\lambda}}$ and the distance from L_v to both borders parallel to L_v is greater than $\frac{1}{\sqrt{\lambda}}$, then (88) holds for a, c and α as in Theorem 4.1 with the additional $C_1 = \frac{\mathbb{P}(\bar{S} \leq \lambda N^{2+\beta})}{\mathbb{P}(K \leq \lambda N^{2+\beta})}$ with $\bar{S} \sim Poi\left(\lambda N(N - \frac{2}{\sqrt{\lambda}})\right)$.

Proof. Assume $t > \frac{a}{\sqrt{\lambda}}$ and the distance from L_v to both parallel borders is at least $\frac{1}{\sqrt{\lambda}}$. Let us consider the setup from the proof of Theorem 4.1 with the adjusted stripe $\tilde{S}_v$ (and $\tilde{S}'_v$ on the other side) of width $\frac{1}{\sqrt{\lambda}}$ and containing $b_t := \lfloor t \cdot \sqrt{\lambda} \rfloor - 2$ boxes. We keep the events $\tilde{B}$ and $\tilde{B}'$ – that the points in the adjusted stripes do not cut off L_v (see (25) and (26)). These events are independent, but not when conditioning on $K \leq \lambda N^{2+\beta}$. However, they are independent of the number of points outside of the stripes S_v and S'_v. This is because points outside of the stripes cannot influence whether a line from a point in the stripes cuts off L_v. The size of the area where the points do influence these events, i.e., the stripes S_v and S'_v, is bounded by $\frac{2t}{\sqrt{\lambda}} \leq \frac{2N}{\sqrt{\lambda}}$. So denote the number of points outside of the stripes

$$\tilde{S} \sim \text{Poi}(\lambda N^2 - 2t\sqrt{\lambda}). \tag{89}$$

The events $\tilde{B}$ and $\tilde{B}'$ are independent of $\tilde{S}$. Furthermore, $\tilde{S} \leq K$ holds because the area which $\tilde{S}$ corresponds to is a subset of Ω, which implies stochastic dominance of K over $\tilde{S}$. We can make the following argument:

$$\begin{aligned}
\mathbb{P}(L_v > t | K \leq \lambda N^{2+\beta}) &\leq \mathbb{P}(\tilde{B} \cap \tilde{B}' | K \leq \lambda N^{2+\beta}) && (90)\\
&= \frac{\mathbb{P}(\tilde{B} \cap \tilde{B}' \cap \{K \leq \lambda N^{2+\beta}\})}{\mathbb{P}(K \leq \lambda N^{2+\beta})} && (91)\\
&\leq \frac{\mathbb{P}(\tilde{B} \cap \tilde{B}' \cap \{\tilde{S} \leq \lambda N^{2+\beta}\})}{\mathbb{P}(K \leq \lambda N^{2+\beta})} && (92)\\
&= \frac{\mathbb{P}(\tilde{S} \leq \lambda N^{2+\beta})}{\mathbb{P}(K \leq \lambda N^{2+\beta})} \mathbb{P}(\tilde{B}) \mathbb{P}(\tilde{B}'), && (93)\\
&\leq C_{1,t} c e^{-\alpha t}, && (94)
\end{aligned}$$

where c and α are as before in Theorem 4.1. To make the factor $C_{1,t} = \frac{\mathbb{P}(\tilde{S} \leq \lambda N^{2+\beta})}{\mathbb{P}(K \leq \lambda N^{2+\beta})}$ independent of t, note that for some $\bar{S} \sim \text{Poi}(\lambda N(N - \frac{2}{\sqrt{\lambda}}))$, it holds that

$$\mathbb{P}(\tilde{S} \leq \lambda N^{2+\beta}) \leq \mathbb{P}(\bar{S} \leq \lambda N^{2+\beta}). \tag{95}$$

So with $C_1 := \frac{\mathbb{P}(\bar{S} \leq \lambda N^{2+\beta})}{\mathbb{P}(K \leq \lambda N^{2+\beta})} \geq C_{1,t}$, the bound is proved.

□

The next step is to find $\mathbb{E}(Y_v)$.

Lemma 4.2. *Let $v \in \mathcal{V}$ be uniformly selected and assume the distance from L_v to the parallel borders is at least $\frac{1}{\sqrt{\lambda}}$. Let $\{L_v \to border\}$ denote the event that the line L_v runs into the border of the box Ω. Then*

$$\mathbb{E}(\mathbb{1}\{L_v \to border\} | K \leq \lambda N^{2+\beta}) \leq \frac{1}{\alpha N} \left(\ln(C_1 c) + 1 - C_1 c e^{-\alpha N}\right) \tag{96}$$

for large N with C_1, c and α like in Lemma 4.1.

We can observe that, as one would expect, the bound decreases in N and intensity λ (as α increases in λ).

Proof. Let d_{border} denote the distance from v to the bound in the direction of growth of L_v. Since the vertices come from a Poisson process, they are uniform in Ω when conditioning on the number of points and thus the distance from the border of Ω is uniformly distributed on $[0, N]$. Denote $\tilde{N} = \min(N, \frac{\ln(C_1 c)}{\alpha})$ which is the minimum value of t where the exponentially decaying bound from Lemma 4.1 is less than or equal to 1. Using the law of total probability and the fact that the number of points and distance from the border are independent, we obtain the following:

$$\begin{aligned}
&\mathbb{E}(\mathbb{1}\{L_v \to \text{border}\} | K \leq \lambda N^{2+\beta}) && (97)\\
&= \mathbb{P}(\{L_v \to \text{border}\} | K \leq \lambda N^{2+\beta}) && (98)\\
&= \int_0^N \frac{1}{N} \cdot \mathbb{P}(\{L_v \to \text{border}\} | K \leq \lambda N^{2+\beta}, d_{\text{border}} = t) dt && (99)\\
&\leq \int_0^{\tilde{N}} \frac{1}{N} \cdot 1 dt + \int_{\tilde{N}}^N \frac{1}{N} \cdot C_1 c e^{-\alpha t} dt && (100)\\
&= \frac{1}{\alpha N} \left(\ln(C_1 c) + 1 - C_1 c e^{-\alpha N}\right). && (101)
\end{aligned}$$

Since the exponential bound for the probability $\mathbb{P}(L_v > t | K \leq \lambda N^{2+\beta})$ in Lemma 4.1 does not assume knowledge or the probability of potential points outside of the stripe, adding the condition of the distance to the border does not change that exponential bound and can be used in the same way for the step with the inequality in (100). □

Now, these lemmas can be combined to complete the proof of Theorem 4.3.

Proof of Theorem 4.3. Fix $\beta > 0$ and let C_1, c and α be defined as in Lemma 4.1. Set $C_2 = \mathbb{P}(K \leq \lambda N^{2+\beta})$. This clearly also depends on the choice of β.

$$\mathbb{E}(Y) = \mathbb{P}(K \leq \lambda N^{2+\beta}) \cdot \mathbb{E}(Y | K \leq \lambda N^{2+\beta}) + \sum_{k > \lambda N^{2+\beta}} \mathbb{E}(Y|K=k) \cdot \mathbb{P}(K=k) \tag{102}$$

$$\leq 2C_2 \lambda N^{2+\beta} \cdot \mathbb{P}(\{L_v \to \text{border}\} | K \leq \lambda N^{2+\beta}) \tag{103}$$

$$+ \sum_{k > \lambda N^{2+\beta}} 2k \cdot \mathbb{P}(\{L_v \to \text{border}\} | K = k) \cdot \mathbb{P}(K=k) \tag{104}$$

$$\leq 2C_2 \lambda N^{2+\beta} \frac{1}{\alpha N} \left(\ln(C_1 c) + 1 - C_1 c e^{-\alpha N} \right) + 2\lambda N^2 \sum_{k > \lambda N^{2+\beta}} \frac{e^{-\lambda N^2} (\lambda N^2)^{k-1}}{(k-1)!} \tag{105}$$

$$\leq 2C_2 \lambda N^{1+\beta} \alpha^{-1} \left(\ln(C_1 c) + 1 - C_1 c e^{-\alpha N} \right) + 2\lambda N^2 \, \mathbb{P}(K \geq \lambda N^{2+\beta}) \tag{106}$$

$$\leq \underbrace{\left(2C_2 \lambda \alpha^{-1} \left(\ln(C_1 c) + 1 - C_1 c e^{-\alpha N} \right) \right)}_{\tilde{C}(\beta)} N^{1+\beta} \tag{107}$$

$$+ 2\lambda N^2 \exp\left(-\lambda N^{2+\beta} (\beta \ln(N) - 1 + N^{-\beta}) \right) \tag{108}$$

The last inequality comes from Theorem 2.1:

$$\mathbb{P}(K \geq \lambda N^{2+\beta}) \leq \exp(\lambda N^{2+\beta} - \lambda N^2) \left(\frac{\lambda N^{2+\beta}}{\lambda N^2} \right)^{\lambda N^{2+\beta}} \tag{109}$$

$$= \exp\left(-\lambda N^{2+\beta} (N^{-\beta} - 1 + \beta \ln(N)) \right). \tag{110}$$

The expression (108) converges to 0 as $N \to \infty$. Hence, $C(\beta)$ can be chosen as an appropriate multiple of $\tilde{C}(\beta)$ to include (108). This concludes the proof. □

Remark 4.3. *It should be noted that the choice of β is crucial for the performance of the bound. For a fixed N, the smaller the β, especially $\beta \approx 0$, the larger $C_1 \geq 1$ and $C_2 \leq 1$. Both C_1 and C_2 converge to 1 as $N \to \infty$. Furthermore, for a fixed $\beta > 0$, the larger N, the smaller the second part of the sum. Finally, choosing β close to zero yields an almost linear bound in N.*

In addition to the upper bound for $\mathbb{E}(Y)$ that can be made arbitrarily close to linear in N for large N, we can also derive a lower bound that is linear in N.

Theorem 4.4. *Let Y be the number of escaping lines and $K \sim Poi(\lambda N^2), \lambda > 0$. Then, there exist constants C_1 and C_2 such that*

$$\mathbb{E}(Y) \geq C_1 N - C_2. \tag{111}$$

Proof. To prove this, the concept that was used to prove Theorem 4.1 can be used: the number of tops in a stripe of width $\frac{1}{\sqrt{\lambda}}$ being bounded by a scaling of the number of filled boxes in the stripe.

Consider a frame of width $\frac{1}{\sqrt{\lambda}}$ in Ω, as illustrated in Figure 22. Cutting away the corner squares, also with side length $\frac{1}{\sqrt{\lambda}}$, leaves the four stripes $S_1, \dots, S_4$ shaded red in that figure. The number of escaping lines is independent for all four stripes. We can again consider tops in those stripes, this time facing the border instead of some line L_v. If a top has orientation orthogonal to the border, it is guaranteed to have an escaping line. This is illustrated in the example stripe S_2 in the figure as well. There, it also becomes apparent that tops are not guaranteed to escape as they might have a line growing parallel to the border. It is also possible for points that are not tops to have escaping lines, in case the top by which it could be blocked has orientation orthogonal to the border. In total, the number of escaping lines from the stripes is bounded from below by the number of tops with orientation opposite of the closest border. Being orthogonal to the border has probability $\frac{1}{2}$ for each point independently.

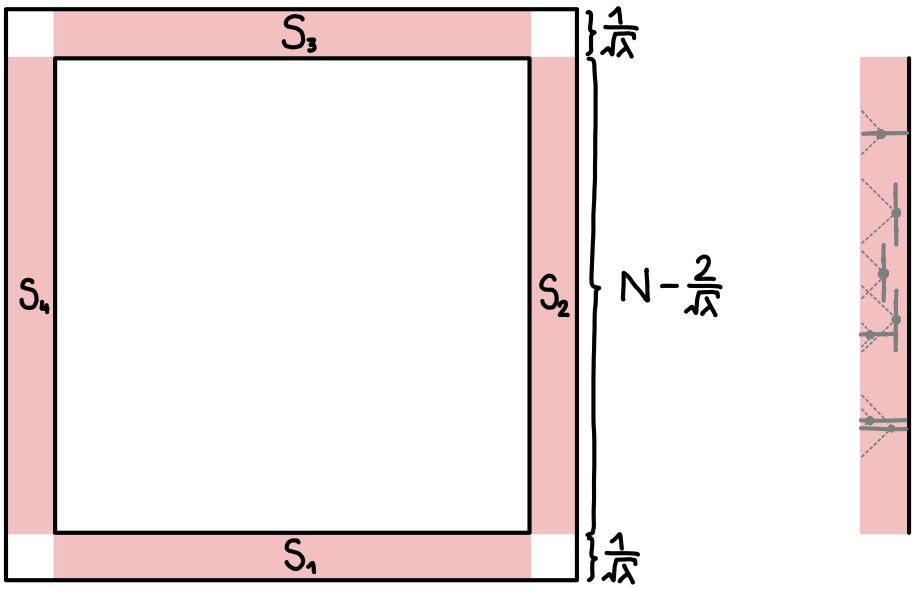

Figure 22: Illustration of the frame of width $\frac{1}{\sqrt{\lambda}}$ and stripes $S_1, \dots, S_4$. On the right side, an example of S_2 with tops and vertices that are not tops whose lines reach the border.

Now consider one stripe and divide it into boxes with side length $\frac{1}{\sqrt{\lambda}}$ again, meaning the number of points in each box follows a Poi(1) distribution independently for all boxes. That also means a box is non-empty with probability $\left(1 - \frac{1}{e}\right)$. This leaves

$$b_t := \left\lfloor \sqrt{\lambda} \left(N - \frac{2}{\sqrt{\lambda}} \right) \right\rfloor \geq \sqrt{\lambda} N - 3 \tag{112}$$

whole boxes. So let M be the number of tops and $\xi \sim \mathrm{Bin}(b_t, 1 - \frac{1}{e})$ be the number of non-empty boxes. Recalling the arguments in the proof of Theorem 4.1, it holds that $M \geq \lfloor \frac{\xi}{3} \rfloor - 2$. The expected value of the number of orthogonal tops is $\frac{1}{2} \cdot \mathbb{E}(M)$ as the orientation is independent of the position of the points. Because there are four stripes,

the following holds:

$$\mathbb{E}(Y) \geq 4 \cdot \frac{1}{2} \cdot \mathbb{E}(M) \tag{113}$$

$$\geq 2\mathbb{E}\left(\left\lfloor \frac{\xi}{3} \right\rfloor - 2\right) \geq 2\mathbb{E}\left(\frac{\xi}{3} - 3\right) \tag{114}$$

$$= \frac{2}{3}\mathbb{E}(\xi) - 6 = \frac{2}{3}(1 - \frac{1}{e})b_t - 6 \tag{115}$$

$$\geq \frac{2}{3}(\sqrt{\lambda}N - 3)(1 - \frac{1}{e}) - 6 \tag{116}$$

$$= \underbrace{\frac{2}{3}\sqrt{\lambda}(1 - \frac{1}{e})}_{C_1} N - \underbrace{(6 + 2(1 - \frac{1}{e}))}_{C_2}, \tag{117}$$

which is linear in N. □

Next, we want to consider the covariance between the growth of lines from different vertices depending on their distance. As described in the observations about the model in Section 3, the potential interaction seems to become increasingly unlikely with growing distance – if that also means the number of points between them increases.

Recall the definition of L_v (see (3.1)) and define

$$Z_v^{(t)} = \mathbb{1}(L_v > t) \tag{118}$$

for some uniformly selected vertex $v \in \mathcal{V}$. Let us consider how far the lines from two vertices can grow independently of each other, for a fixed distance between them. First, define a useful metric.

Definition 4.2 (Distance between vertices)**.** *Let $u, v \in \mathcal{V}$. Define*

$$d(u, v) = \|u - v\|_1 = |u_1 - v_1| + |u_2 - v_2| \tag{119}$$

through the p-norm with $p = 1$ as the distance between u and v. Denote $d_1(u, v) = |u_1 - v_1|$ and $d_2(u, v) = |u_2 - v_2|$ as the distances in the x- and y-coordinates.

With this, we can consider different cases of L_u and L_v for different orientations of u and v. These are shown in Figure 23, where the distance between them is fixed. The first row displays the case where the vertices have the same orientation, which is also parallel to the direction of the maximum of $d_1(u, v)$ and $d_2(u, v)$. The second row is similar, but they are growing parallel to the shorter distance. In these two cases, where they grow parallel, cases (i) and (ii) are the same up to flipping. The third row presents the possibilities for when they are orthogonal. Clearly, which vertex is horizontal and which is vertical could be switched, but that results in the same type of possibilities.

Table 1 shows the different maximum possible t in $\{L_u > t\}$ and $\{L_v > t\}$ such that these events are independent, which can be derived from Figure 23. This is when the

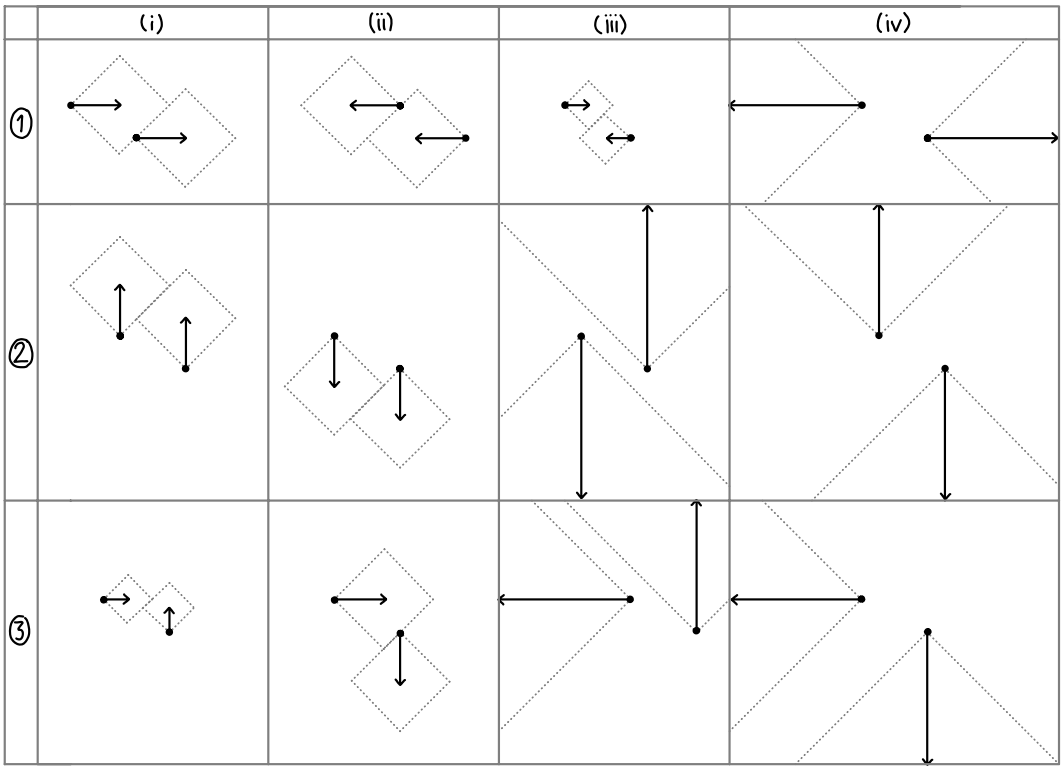

Figure 23: Illustration of the different cases of L_u and L_v for a fixed distance between the vertices. The diamonds have the maximum possible equal size for the independent growth of the corresponding lines.

areas of influence D_v and D_u do not overlap, as illustrated in the figure. The following lemma draws a general conclusion from this.

	(i)	(ii)	(iii)	(iv)
(1)	$t \leq \frac{1}{2}d(u,v)$	$t \leq \frac{1}{2}d(u,v)$	$t \leq \frac{1}{4}d(u,v)$	$\forall t > 0$
(2)	$t \leq \frac{1}{2}d(u,v)$	$t \leq \frac{1}{2}d(u,v)$	$\forall t > 0$	$\forall t > 0$
(3)	$t \leq \frac{1}{4}d(u,v)$	$t \leq \frac{1}{2}d(u,v)$	$\forall t > 0$	$\forall t > 0$

Table 1: Distances of how far lines from two vertices can grow independently for the cases corresponding to 23.

Lemma 4.3. *For any L_u and L_v of uniformly selected $u, v \in \mathcal{V}$, the events $\{L_u > t\}$ and $\{L_v > t\}$ are independent for all $t \leq \frac{1}{4}d(u,v)$.*

Proof. This follows from Table 1. □

This lemma is central for the next theorem.

Theorem 4.5. *Select two vertices $u, v \in \mathcal{V}$ uniformly. Then there are constants c and α such that the following bound holds for the covariance between $Z_u^{(t)}$ and $Z_v^{(t)}$ for all t:*

$$|Cov(Z_u^{(t)}, Z_v^{(t)})| \leq c^2 e^{-\frac{\alpha}{2}d(u,v)}. \tag{120}$$

In particular, if $d(u,v) > \frac{4a}{\sqrt{\lambda}}$, *then* (120) *holds for the values of* a, c *and* α *from Theorem* 4.1.

Proof. Assume $d(u,v) > \frac{4a}{\sqrt{\lambda}}$. First, observe that, for any $\tilde{t} \in (0,t)$, the event $\{L_v > t\}$ can be rewritten as follows:

$$\{L_v > t\} = \{L_v > \tilde{t}\} \cap \{L_v \text{ not cut off in } [\tilde{t}, t]\}. \tag{121}$$

For shorter notation, denote $\{L_v \text{ not cut off in } [\tilde{t}, t]\}$ by $\{L_v \text{ surv. } [\tilde{t}, t]\}$. Because of Lemma 4.3, choose

$$\tilde{t} = \frac{1}{4} d(u,v), \tag{122}$$

and note that then,

$$\mathbb{P}(L_u > \tilde{t} | L_v > \tilde{t}) = \mathbb{P}(L_u > \tilde{t}). \tag{123}$$

Finally, use Theorem4.1 for the last inequality.

$$\begin{aligned}
&\left|\mathrm{Cov}(Z_u^{(t)}, Z_v^{(t)})\right| = \left|\mathbb{P}(L_u > t, L_v > t) - \mathbb{P}(L_u > t)\mathbb{P}(L_v > t)\right| && (124)\\
&= \Big|\mathbb{P}(L_v \text{ surv. } [\tilde{t}, t] | L_u \text{ surv. } [\tilde{t}, t], L_v > \tilde{t}, L_u > \tilde{t}) \cdot \\
&\qquad \mathbb{P}(L_u \text{ surv. } [\tilde{t}, t] | L_v > \tilde{t}, L_u > \tilde{t}) \cdot \mathbb{P}(L_u > \tilde{t} | L_v > \tilde{t}) \cdot \mathbb{P}(L_v > \tilde{t}) && (125)\\
&\qquad\quad - \mathbb{P}(L_v \text{ surv. } [\tilde{t}, t] | L_v > \tilde{t}) \cdot \mathbb{P}(L_v > \tilde{t}) \cdot \mathbb{P}(L_u \text{ surv. } [\tilde{t}, t] | L_u > \tilde{t}) \cdot \mathbb{P}(L_u > \tilde{t})\Big| \\
&= \left|\mathbb{P}(L_u > \tilde{t})\mathbb{P}(L_v > \tilde{t})\right| \cdot \\
&\quad \Big|\mathbb{P}(L_v \text{ surv. } [\tilde{t}, t] | L_u \text{ surv. } [\tilde{t}, t], L_v > \tilde{t}, L_u > \tilde{t}) \mathbb{P}(L_u \text{ surv. } [\tilde{t}, t] | L_v > \tilde{t}, L_u > \tilde{t}) && (126)\\
&\qquad - \mathbb{P}(L_u \text{ surv. } [\tilde{t}, t] | L_u > \tilde{t}) \mathbb{P}(L_v \text{ surv. } [\tilde{t}, t] | L_v > \tilde{t})\Big| \\
&\leq \mathbb{P}(L_u > \tilde{t})\mathbb{P}(L_v > \tilde{t}) && (127)\\
&\leq c^2 e^{-\frac{\alpha}{2} d(u,v)} && (128)
\end{aligned}$$

□

Of course, some cases of L_u and L_v have even weaker covariance or are in fact independent because the areas of influence do not overlap no matter how far they grow. However, the theorem stated above holds for all cases presented in Table 1 and Figure 23.

This theorem bounded the absolute value of the covariance, but it is also interesting to know about the sign of the covariance. We have the following conjecture.

Conjecture 4.1. *Consider* $Z_u^{(t)}$ *and* $Z_v^{(t)}$ *for uniformly selected* $u, v \in \mathcal{V}$ *and direction of growth. The following holds for the sign of the covariance:*

$$Cov(Z_u^{(t)}, Z_v^{(t)}) \begin{cases} \geq 0 & \text{if } u, v \text{ have the same orientation,} \\ \leq 0 & \text{if } u, v \text{ are orthogonal.} \end{cases} \tag{129}$$

Inspect the two cases more closely by considering some illustrations. Figure 24 shows two examples of some L_u and L_v where they are parallel. We can split

$$\begin{aligned} \mathrm{Cov}(Z_u^{(t)}, Z_v^{(t)}) &= \mathbb{P}(L_u > t, L_v > t) - \mathbb{P}(L_u > t)\,\mathbb{P}(L_v > t) && (130) \\ &= \mathbb{P}(L_u > t | L_v > t)\,\mathbb{P}(L_v > t) - \mathbb{P}(L_u > t)\,\mathbb{P}(L_v > t) && (131) \end{aligned}$$

and consider $\mathbb{P}(L_u > t | L_v > t)$. In the left illustration in Figure 24, there are shaded areas, which we now call *protected areas* because of the following. When conditioning on $L_v > t$, i.e., the grey line growing at least as far as depicted in the figure, no points in the area shaded blue can cut off L_u as they cannot pass the grey line. There are two reasons why the impact of this decreases with increasing distance between u and v. One is that the further away L_u and L_v are, the more points there are between the lines and that makes it more likely that that lines from points in the shaded areas would have no impact, because they are more likely to be cut off. Furthermore, the larger the distance between u and v, the smaller these areas become. Still, these arguments lead to the conjecture that the covariance is positive for parallel lines. However, it is more difficult to say when the lines do not have these protected areas, as illustrated in the right figure.

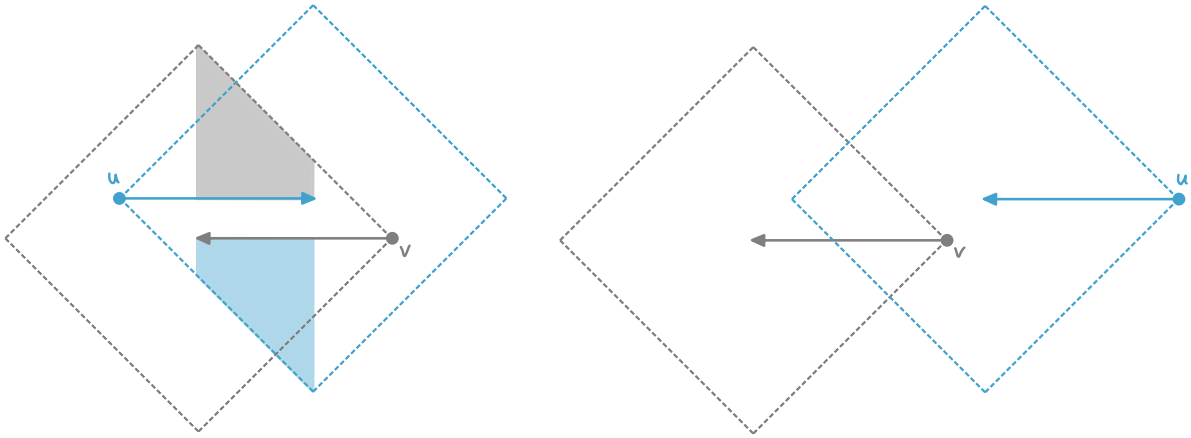

Figure 24: Illustration of *protected* areas on the left and weak overlapping of the diamonds D_v and D_u on the right.

This looks very different when the lines grow orthogonal to each other. The left illustration in Figure 25 shows that if a point u is in the cone $C_v^{(t)}$ and grows towards the line L_v, it is impossible for both to grow larger than t, i.e., $\mathbb{P}(L_v > t, L_u > t) = 0$. Thus the covariance is negative in that case. But like in the parallel scenario, it is more difficult to say something about the covariance when the diamonds, and especially the cones, barely overlap, like in the right illustration in the figure.

Generally, it is important to realise that this covariance structure strongly depends on the assumption that $K \sim \mathrm{Poi}(\lambda N^2)$, specifically on the fact that the expected number of

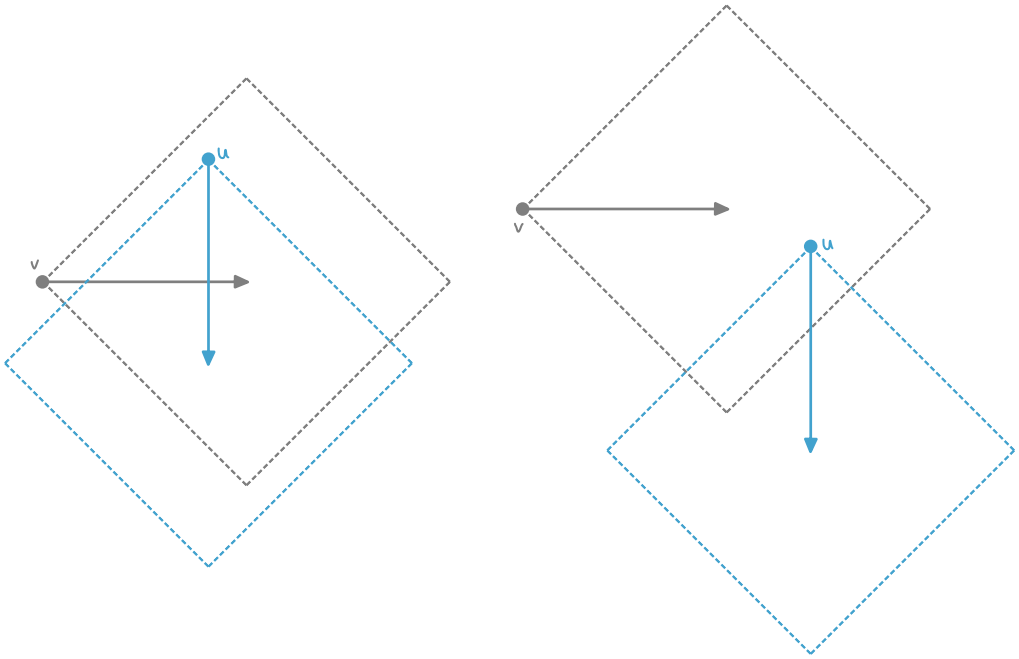

Figure 25: Illustration of the argument for (possibly) negative covariance.

points in Ω increases for increasing t and tends to infinity for $N \to \infty$. There are more details on this assumption in the next subsection.

To understand this better, consider the case of two points in Ω, regardless of the size of Ω. No matter their distance, there is a probability of $\frac{1}{2}$ that they collide, as that happens with probability one in the case that they are not parallel. This means that there is no decay in the covariance regarding their distance. This leads to the question when, i.e., for what intensities, there is exponential decay in covariance and motivates to generalise the model as follows.

4.2 Changing the Poisson Intensity

Another possible assumption for the intensity on Ω is to consider intensities depending on N, for example $\Lambda(N) = \frac{\lambda}{N^2}$ for some $\lambda > 0$, i.e., expecting λ points in the square, no matter the size of it. Then the behaviour of the probability $\mathbb{P}(L_v > t)$ might change and no longer show exponential decay. Similarly, if $\Lambda(N) = \frac{\lambda}{N^\beta}$ for some $\beta < 2$, the number of expected points in Ω still grows with increasing N, but the larger β, the slower the increase. Let us consider $\Lambda(N) = \frac{\lambda}{N^\beta}$ for $\beta < 2$ next.

Proposition 4.2. *Let $\lambda > 0$ be fixed and denote $\Lambda(N) = \frac{\lambda}{N^\beta}$ for $\beta < 2$ fixed. So $K \sim Poi(\Lambda(N) \cdot N^2) = Poi(\lambda N^{2-\beta})$. Then there exist constants c and α such that, for all t and N,*

$$\mathbb{P}(L_v > t) \leq ce^{-\alpha t}. \tag{132}$$

In particular, if $t > \frac{a}{\sqrt{\Lambda(N)}}$ *and the distance to both borders parallel to* L_v *is greater than* $\frac{1}{\sqrt{\Lambda(N)}}$*, then (132) holds for* $\alpha = \frac{\sqrt{\lambda}\vartheta_{opt}^2}{N^{\beta/2}}(1-\frac{1}{e})$ *and* a, ϑ_{opt} *and* c *remain unchanged from Theorem 4.1.*

Remark 4.4. *This theorem indicates that the behaviour of exponential decay still exists for such a* $\Lambda(N)$*. The closer* β *is to 0, i.e., the closer it is to the model with constant intensity and* $K \sim Poi(\lambda N^2)$*, the stronger the exponential decay. The reverse also holds: the closer* β *to 2, the slower the exponential decay. If* $\beta < 0$*, then the decay is even stronger than for the model with constant intensity discussed in the previous subsection.*

Proof. The proof of this is only outlined as it works in the same way as the original theorem's proof. What is changed is that now, the length of the squares in the stripe needs to be adjusted to $\frac{N^{\beta/2}}{\sqrt{\lambda}}$ and so there are $b_t = \left\lfloor t \cdot \frac{\sqrt{\lambda}}{N^{\beta/2}} \right\rfloor - 2$ boxes. So we have $\xi \sim \text{Bin}(b_t, 1-\frac{1}{e})$ as before but with adjusted λ and b_t. Plugging this into the original proof yields the α stated in this theorem. □

Considering the theorems presented so far gives way to think more carefully about how to interpret expressions like $t \to \infty$ (for example in Theorem 4.1) or $d(u,v) \to \infty$ (in Theorem 4.5). When the model is defined on $\Omega = [0,N]^2$ and $K \sim \text{Poi}(\lambda N^{2-\beta})$, $\beta < 2$, then $N \to \infty$ is necessary for $t \to \infty$ to be possible, as $t \leq N$. This suggests looking at $t \to \infty$ by setting $t = t(N) = \delta N$ for a fixed $\delta \in (0,1)$, and then $N \to \infty$. This also provides a way to approach the question of a phase transition of the behaviour of this model for $\beta \geq 2$.

Let us consider $K \sim \text{Poi}(\lambda N^{2-\beta})$ for any β and investigate $\mathbb{P}(L_v > t)$ for $t = t(N) = \delta N$ and $N \to \infty$. We obtain the following from Proposition 4.2:

$$\mathbb{P}(L_v > t) \leq c \exp\left(-\frac{\vartheta_{\text{opt}}^2\sqrt{\lambda}}{N^{\beta/2}}(1-\frac{1}{e})t\right) \tag{133}$$

$$= c \exp\left(-\frac{\vartheta_{\text{opt}}^2\sqrt{\lambda}\delta}{N^{\beta/2-1}}(1-\frac{1}{e})\right) \tag{134}$$

From this we can observe that, when $\beta = 2$, the upper bound remains constant for $N \to \infty$, while for $\beta < 2$, there is exponential decay (even if it is slow for large β). For $\beta > 2$, there is exponential growth, which does not yield an interesting scenario. The question is whether the exact probability behaves the same way. Let us investigate the lower bound for that.

As the lower bound in Theorem 4.2 also decays exponentially in $\sqrt{\lambda}t$ for $\beta < 2$, it can be adjusted for $\Lambda(N) = \frac{\lambda}{N^\beta}$ like Proposition 4.2 for Theorem 4.1. The bound becomes constant in N for $\beta = 2$ when replacing the intensity by $\Lambda(N) = \frac{\lambda}{N^2}$ and $t = \delta N$, in the same way the upper bound does. This means that both the upper and lower bound do not

display exponential decay for $t(N) \to \infty$ and hence, $\mathbb{P}(L_v > t)$ cannot decay exponentially for $N \to \infty$ either.

All these arguments imply that $\beta = 2$ is a critical point and marks a phase transition for $\mathbb{P}(L_v > t)$ when $t = t(N) \to \infty$.

Another way to approach our model is to disregard the size of the box, set it to $[0,1]^2$, and make the assumption that there are $K \sim \text{Poi}(\lambda)$ points. The question of $\mathbb{P}(L_v > t)$ from earlier can then be considered from the angle of increasing the intensity λ instead of the distance t to detect exponential decay. That is because of the following connection.

When considering $\Omega = [0,N]^2$, the crucial part that is responsible for the exponentially decaying probability of L_v growing further is that there are increasingly many points that might cut it off. So that can be re-scaled to fixing the distance t in $\mathbb{P}(L_v > t)$ and increasing the intensity of the Poisson process. In more detail, this is represented by the following proposition, for which we consider a two-dimensional Poisson process on $[0,1]^2$.

Proposition 4.3. *Let $K \sim Poi(\lambda), \lambda > 1$, the Poisson process on $[0,1]^2$. Let $t \in (0,1)$ be fixed. Then there exist constants c and α such that*

$$\mathbb{P}(L_v > t) \leq ce^{-\alpha\sqrt{\lambda}} \tag{135}$$

for all λ. In particular, if $\sqrt{\lambda} > \frac{a}{t}$ this holds for $\alpha = \vartheta_{opt}^2(1-\frac{1}{e})t$ with ϑ_{opt}, c and a like in Theorem 4.1.

Proof. This proof is only outlined again as most of it works exactly like in Theorem 4.1. The side length of the squares in the stripe S_v is kept as $\frac{1}{\sqrt{\lambda}}$ so that there are Poi(1) points independently in each of the $b_t = \lfloor t \cdot \sqrt{\lambda} \rfloor - 2$ boxes. Also, $\xi \sim \text{Bin}(b_t, 1-\frac{1}{e})$ as before. The bound and the constant c are the same, and the perspective here is to increase λ. Then $\mathbb{P}(L_v > t) \to 0$ as $\lambda \to \infty$ with $\alpha = \vartheta_{\text{opt}}^2(1-\frac{1}{e})t$. □

Remark 4.5. *It should be noted that, when changing the intensity regardless of the size of the box, i.e., changing the constant λ, the size of the box does not matter. It is then just a question of scaling whether we consider $[0,1]^2$ or $[0,N]^2$. Choosing $[0,N]^2$ and considering decay in distance instead of intensity provides a way to quantify the speed of growth and decay.*

The scaling and how the models on $[0,1]^2$ and $[0,N]^2$ relate can be made precise. Let $L_{v,\lambda,N}$ be defined like in Definition 3.1, only that λ and N in the index indicate that it corresponds to constant intensity λ and the size of Ω being N, i.e., $K \sim \text{Poi}(\lambda N^2)$ points in $[0,N]^2$. With the above definitions it holds that

$$L_{v,\lambda,N} \overset{d}{=} \frac{1}{\sqrt{\lambda}} L_{v,1,\sqrt{\lambda}N}. \tag{136}$$

The upper bound in Theorem 4.1 and the lower bound in Theorem 4.2 each coincide for $\mathbb{P}(L_{v,\lambda,N} > t)$ and $\mathbb{P}(\frac{1}{\sqrt{\lambda}} L_{v,1,\sqrt{\lambda}N} > t) = \mathbb{P}(L_{v,1,\sqrt{\lambda}N} > \sqrt{\lambda}t)$ for some fixed $t \leq N$. This is because the crucial part for the exponential decay is the Poisson intensity, specifically in C_v and D_v. The expected number of points in $[0, N] \times [0, N]$ with intensity parameter λ is λN^2, as well as on $[0, \sqrt{\lambda}N] \times [0, \sqrt{\lambda}N]$ with intensity parameter 1. Furthermore, the Poisson intensity for the area of influence, $D_v^{(t)}$ for $\{L_{v,\lambda,N} > t\}$ and $D_v^{(\sqrt{\lambda}t)}$ for $\{L_{v,1,\sqrt{\lambda}N} > \sqrt{\lambda}t\}$ respectively, is the same for each diamond, which is $2\lambda t^2$.

The phenomenon on phase transition at $\beta = 2$ for $K \sim \text{Poi}(\lambda N^{2-\beta})$ also becomes apparent when considering this question in the light of the relationship between the model on $[0, 1]^2$ and changing λ or $[0, N]^2$ with $\Lambda(N) = \frac{\lambda}{N^\beta}$ and increasing N and $t(N)$. When $\beta = 2$, the distribution of the number of points in Ω does not change, and this is equivalent to keeping λ constant in the setup on $[0, 1]^2$ and not changing t, which clearly cannot show any decay then. Generally, the two model definitions can be considered equivalently, only that $\lambda(N) = \frac{\lambda}{N^\beta}, \beta < 2$, on $[0, N]^2$ gives a rate of change in the intensity of the Poisson distribution parameter.

5 Other Characteristics and Phenomena

There are many questions and ideas for generalisations that come up when working on this model. Some of them are explored in this chapter.

5.1 Rectangles

A part that was not explored in detail is the characteristics connected to the number, area and side length of the rectangles yielded from this process.

Proposition 5.1. *Let $K \sim Poi(\lambda)$ be the number of points in $\Omega = [0, 1]^2$ and let R be the number of rectangles. Then $\mathbb{E}(R) = \lambda + 1$.*

Proof. Assume that there are initially $K = k$ points in Ω. Let us call the event of one line running into another line *collision*. We observe that

$$\#\{\text{collisions}\} + \#\{\text{escaping lines}\} = 2k. \tag{137}$$

This is because each point grows two lines and each line ends either by colliding with another line or because it runs into the bound of the box. Furthermore, each collision stops almost surely only one line.

Next, we observe that the corner of a rectangle is either a collision of a line with another one or with the boundary of the box. And in four cases, it is a corner of $[0, 1]^2$. Unless it is a corner of Ω, such a point makes one corner for two rectangles, and each

rectangle has four corners. Thus, the points of collisions with other lines or the bound make k rectangles. There is one additional rectangle from the corners of Ω.

All in all, it then holds $\mathbb{E}(R) = \mathbb{E}(K+1) = \lambda + 1$. □

This also matches the well-known Euler's formula about the relationship of the number of vertices (V), edges (E) and faces (F) for planar graphs, which states that $V - E + F = 2$. Here, the vertices are all corners of the rectangles, which, in the case of k points in Ω, is $V = 2k + 4$ as argued previously. Furthermore, all the vertices are of degree 3, i.e., are connected to 3 edges, except for the four corners of Ω which are of degree 2. This means there are $E = \frac{3}{2}V - 2$ edges. Plugging this into the formula, we obtain $F = k + 2$. As the area outside of Ω is also counted as a face, this leaves $k + 1$ rectangles inside of Ω as stated in the proof.

Generally, the rectangles and their side lengths can be used to pose interesting questions. First, it should be noted that the side lengths of rectangles and the line lengths from certain vertices are not the same – the former depend on the places of collisions between two lines or a line and the border. One can pose the following question. When colouring all rectangles blue, that have a side that is longer than some x_0, and considering this quadrangulation on the entire $\mathbb{R}^2$, is there some critical point x_0 for which there exists almost surely an infinite cluster of blue rectangles? This is a question typical for the field of percolation.

5.2 Models with Alternative Orientation Distributions

How does the model behave when the probability for vertical and horizontal orientation is not $\frac{1}{2}$ each? Let $p > \frac{1}{2}$ be the probability for, say without loss of generality, vertical (or "dominant") orientation and $(1 - p)$ correspondingly the probability for horizontal orientation. Let $\phi_v = \mathbb{1}(v \text{ vertical})$ be the variable denoting the orientation of the vertex v. Then

$$\mathbb{P}(L_v > t) = \mathbb{P}(L_v > t|\phi_v = 1)\mathbb{P}(\phi_v = 1) + \mathbb{P}(L_v > t|\phi_v = 0)\mathbb{P}(\phi_v = 0) \tag{138}$$

$$= \mathbb{P}(L_v > t|\phi_v = 1)p + \mathbb{P}(L_v > t|\phi_v = 0)(1 - p) \tag{139}$$

and, using the definition for $\tilde{B}$ from (25), $i \in \{0, 1\}$:

$$\mathbb{P}(L_v > t|\phi_v = i) \leq \left(\mathbb{P}(\tilde{B}|\phi_v = i)\right)^2. \tag{140}$$

We can focus on the following. What changes is the probability for the points being parallel to the growing line, changing from $\frac{1}{2}$ to p if v is vertical and $(1 - p)$ if it is

horizontal. Additionally, the choice of optimal ϑ is now

$$\vartheta_{\text{opt}}^{(p)} = \frac{\ln(p)}{3} + \sqrt{\frac{\ln(p)^2}{9} - \frac{2}{3}\ln(p)} \tag{141}$$

if v is vertical and

$$\vartheta_{\text{opt}}^{(1-p)} = \frac{\ln(1-p)}{3} + \sqrt{\frac{\ln(1-p)^2}{9} - \frac{2}{3}\ln(1-p)} \tag{142}$$

if v is horizontal. Using all definitions and variables from Theorem 4.1, the following holds for a point with dominant orientation. Some steps that are exactly as in Theorem 4.1 are omitted.

$$\mathbb{P}(\tilde{B}|\phi_v = 1) = \sum_{m=0}^{\infty} \mathbb{P}(\tilde{B}|M = m, \phi_v = 1)\,\mathbb{P}(M = m, \phi_v = 1) \tag{143}$$

$$= \sum_{m=0}^{\gamma} \mathbb{P}(\tilde{B}|M = m, \phi_v = 1)\,\mathbb{P}(M = m) + \sum_{m=\gamma+1}^{\infty} \mathbb{P}(\tilde{B}|M = m, \phi_v = 1)\,\mathbb{P}(M = m) \tag{144}$$

$$\leq \mathbb{P}(M \leq \gamma) + \sum_{m=\gamma+1}^{\infty} p^m \leq \dots \tag{145}$$

$$= \exp\left(-\frac{1}{2}\vartheta^2(1-\frac{1}{e})(t\cdot\sqrt{\lambda}-3)\right) + \exp\left(\frac{\ln(p)}{3}(1-\vartheta)(1-\frac{1}{e})(t\cdot\sqrt{\lambda}-3) - 3\ln(p)\right) \tag{146}$$

$$= \underbrace{\left(\exp\left(\frac{3}{2}(1-\frac{1}{e})(\vartheta_{\text{opt}}^{(p)})^2\right) + p^{-(3+(1-\vartheta_{\text{opt}}^{(p)})(1-\frac{1}{e}))}\right)}_{=:\tilde{c}_1} \cdot \exp\left(-\underbrace{\frac{\sqrt{\lambda}(\vartheta_{\text{opt}}^{(p)})^2}{2}(1-\frac{1}{e})}_{=:\tilde{\alpha}_1} t\right) \tag{147}$$

Using the same idea and considering a point with non-dominant orientation, it holds that:

$$\mathbb{P}(\tilde{B}|\phi_v = 0) = \sum_{m=0}^{\infty} \mathbb{P}(\tilde{B}|M = m, \phi_v = 0)\,\mathbb{P}(M = m) \tag{148}$$

$$\leq \mathbb{P}(M \leq \gamma) + \sum_{m=\gamma+1}^{\infty} (1-p)^m \leq \dots \tag{149}$$

$$= \exp\left(-\frac{1}{2}\vartheta^2(1-\frac{1}{e})(t\cdot\sqrt{\lambda}-3)\right) + \exp\left(\frac{\ln(1-p)}{3}(1-\vartheta)(1-\frac{1}{e})(t\cdot\sqrt{\lambda}-3) - 3\ln(1-p)\right) \tag{150}$$

$$= \underbrace{\left(\exp\left(\frac{3}{2}(1-\frac{1}{e})(\vartheta_{\text{opt}}^{(1-p)})^2\right) + (1-p)^{-(3+(1-\vartheta_{\text{opt}}^{(1-p)})(1-\frac{1}{e}))}\right)}_{=:\tilde{c}_2} \cdot \exp\left(-\underbrace{\frac{\sqrt{\lambda}(\vartheta_{\text{opt}}^{(1-p)})^2}{2}(1-\frac{1}{e})}_{=:\tilde{\alpha}_2} t\right). \tag{151}$$

We obtain the constants $c_1 = \tilde{c}_1^2$, $c_2 = \tilde{c}_2^2$, $\alpha_1 = 2\tilde{\alpha}_1$ and $\alpha_2 = 2\tilde{\alpha}_2$ as before, where c_1 and α_1 are the constants of the exponentially decaying bound of $\mathbb{P}(L_v > t)$ for a vertex v with dominant orientation and c_2 and α_2 the corresponding ones if v has the non-dominant orientation.

As intuition also indicates, the decay is slower if a vertex has the dominant orientation and quicker if it does not as there are less/more points with a "threatening" orientation. Furthermore, when considering the entire $\mathbb{P}(L_v > t)$ (see (139)), so the weighted average of the two cases (which comes from the law of total probability), the overall exponential decay becomes weaker with p closer to 0 or 1 instead of $\frac{1}{2}$.

This can be used to explore how the exponential decay of the covariance changes. The bound from Theorem 4.5 becomes the following:

$$|\mathrm{Cov}(Z_u, Z_v)| \leq \begin{cases} c_1^2 e^{\frac{\alpha_1}{2} d(u,v)}, & \text{if } u, v \text{ vertical,} \\ c_1 c_2 e^{\frac{\alpha_1+\alpha_2}{4} d(u,v)}, & \text{if } u \text{ vertical, } v \text{ horizontal, or vice versa,} \\ c_2^2 e^{\frac{\alpha_2}{2} d(u,v)}, & \text{if } u, v \text{ horizontal.} \end{cases} \tag{152}$$

For a bound that is not separated into these three different cases, use (139) with the obtained bounds. This gives:

$$|\mathrm{Cov}(Z_u, Z_v)| \leq \left(p c_1 e^{-\frac{\alpha_1}{4} d(u,v)} + (1-p) c_2 e^{-\frac{\alpha_2}{4} d(u,v)} \right)^2 \tag{153}$$

$$= p^2 c_1^2 e^{-\frac{\alpha_1}{2} d(u,v)} + 2p(1-p) c_1 c_2 e^{-\frac{\alpha_1+\alpha_2}{4} d(u,v)} + (1-p)^2 c_2^2 e^{-\frac{\alpha_2}{2} d(u,v)}. \tag{154}$$

As observed earlier, for large p, the rate of decay α_1 becomes very small, and that case contributes more to the entire covariance, meaning the exponential decay becomes weaker for p close to 1 (and analogously to 0). This matches intuition, too. When there are a lot of parallel lines, they are more likely to grow much further and thus interfere with the growth of other lines (of both orientations), even if they are further away. All in all, this bound has the strongest rate of decay for $p = \frac{1}{2}$. The same analysis can be done for the lower bound.

Another alternative to consider (which does not originate from [4]) is to allow any orientation on the circle with uniform distribution (see also Section 6). The first thing to realise is that then, two lines are parallel with probability 0, meaning in an infinitely large box, the lines from two points collide at some point with probability 1. Furthermore, the idea of the proof in Theorem 4.1 about the exponential decay of $\mathbb{P}(L_v > t)$ does not work the same way because the concept of points lying inside areas blocked by lines from other points is not as straight forward. In addition, the area of direct influence is no longer a cone but a circle. This is because the distance which a point can have from v to cut off L_v is now different due to the different angles, illustrated in Figure 26. Whether a point is a top does not necessarily just depend on the other points in the same and neighbouring

box but possibly – even if unlikely – on points with much larger distances, also illustrated in the figure.

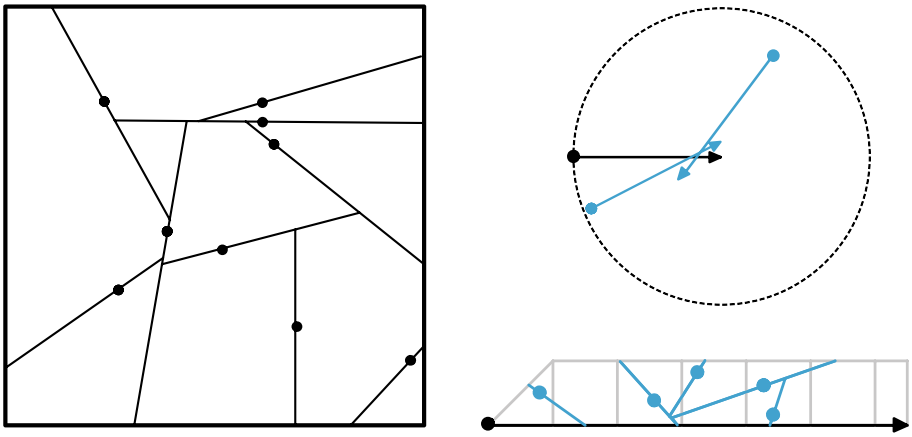

Figure 26: Example of a realisation for angle of orientation uniform on the circle on the left side. Illustration of the area of direct influence on the top right. Illustration that the approach with boxes in the stripe does not work as before on the bottom right.

Another type of behaviour that can be observed for a certain set of activation conditions in Model (b) in Section 3.6 in [4] corresponds to growing lines in both horizontal and both vertical directions from all points of the Poisson process on Ω. Two examples for four and nine vertices are shown in Figure 27. The behaviour is changed in quite some ways.

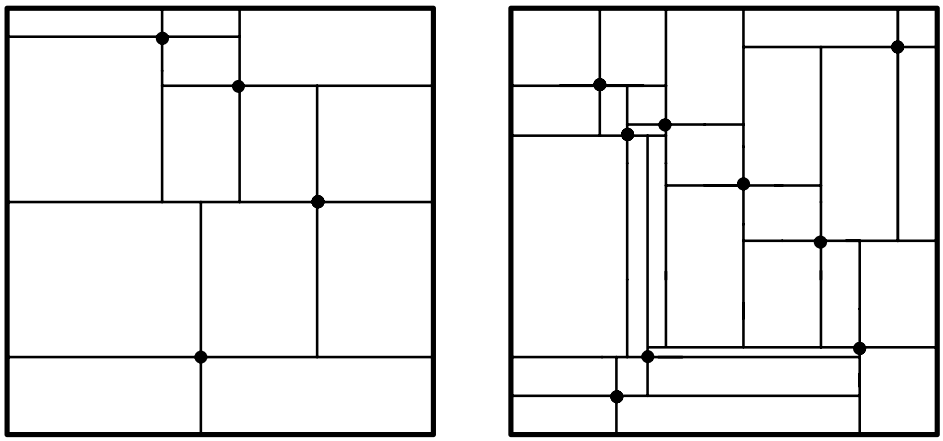

Figure 27: Example with 4 and 9 vertices when all points grow lines in all four directions.

For $\{L_v > t\}$ to happen, the conditions are now much stronger as every point has a line growing in a direction that is a "threat" to L_v. It is a necessary condition that there are no points in $D_v^{(t/2)}$, which has area $t^2/4$. Note that this diamond has only $t/2$ distance between corners and centres (see area shaded red in Figure 28). This is because in that area, lines from points in there can only be stopped by lines from points that are threats themselves. In the remaining area of the cone, it is possible for points to be blocked by

lines from points outside of C_v, illustrated in Figure 28, meaning they can potentially be stopped. Thus a sufficient condition is that there are no points in C_v, which has area t^2. Let K_D be the number of points in $D_v^{(t/2)}$ and K_C in C_v. This yields a lower and upper bound for $\mathbb{P}(L_v > t)$ of the following type:

$$\mathbb{P}(L_v > t) \geq \mathbb{P}(K_C = 0) = e^{-\lambda t^2}, \tag{155}$$

$$\mathbb{P}(L_v > t) \leq \mathbb{P}(K_D = 0) = e^{-\lambda t^2/4}. \tag{156}$$

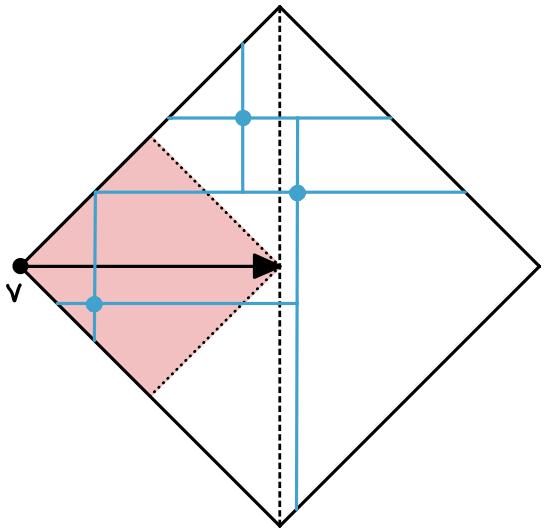

Figure 28: Illustration of the necessary and sufficient conditions for $\{L_v > t\}$, area shaded in red indicates $D_v^{(t/2)}$

It is clear that this decay is much stronger than when the lines grow only horizontally or vertically, as the decay is in t^2 instead of t. Because of this, the decay of the covariance in distance between vertices is also much stronger.

6 Gilbert Tessellation

There are three publications [1], [2], [12] known to the author that have results directly related to the model of this work. All of them agree on the fact that deriving any exact results on our model is highly involved and that the model is to date intractable. The publications work without the restriction that Ω is a finite square, but rather $\Omega = \mathbb{R}^2$ (except for simulations). The latter two also derive results for different proportions of horizontal and vertical lines (as suggested in Section 5.2 in this work). Different approximations are presented in the different articles, as well as simulation results, which are presented and discussed in this section.

The first published work "Homogeneous Rectangular Tessellations" by Mackisack and Miles in 1996 [12] presents this model as a special case of the general model known under

the name of *Gilbert Tessellation*, among some other rectangular tessellations. In the general Gilbert tessellation, the model corresponds to the idea presented in Figure 27, where the lines grow uniformly in any angle on the entire circle. This dates back to work by Edgar Gilbert in 1967 [7], who did not pay particular attention to the case of only horizontal and vertical lines, which results in a quadrangulation. It should be noted that Gilbert is a very well-known mathematician, who introduced a random graph model in 1959 [6]. This is very closely related to the famous Erdős-Renyi model, introduced in 1959 by Erdős and Rényi [5]. The two models were introduced independently.

In [12], an approximate result on the expected value of the line length from one vertex is derived for the rectangular Gilbert tessellation. This is done by using a heuristic approach suggested by Gilbert, based on a mean-field analysis. They obtain the approximate expected value $2.828\sqrt{\lambda}$ (in (39) in [12]) for the mean value per unit area for the total line length. From their approximations, one can also obtain the approximate expected value $2\sqrt{2/\lambda}$ for $\mathcal{L}_v$, i.e., the entire line from some vertex $v \in \mathcal{V}$ for the finished process. It should be noted that this cannot be used entirely equivalently for our model, as there is some bias due to the interactions with the border of Ω in our case. This bias is explored in a simulation study ([12], Section 9-11), but only for one Poisson intensity on a square ($\lambda = 256$) for 50 replicates. So it is not possible to draw a conclusion for a general case. Our work on the tail bounds for the distribution of the line length makes it possible to bound the impact of the bias induced by the border for any intensity. From their study, Mackisack and Miles also conclude that the rectangles have a tendency to be more narrow than a square, i.e., have two longer and two shorter sides, as we observed in Figure 7.

The succeeding work by Burridge, Cowan, and Ma in 2013 [2] improves the approximation of the expected value of the line length, based on an improved algorithm for simulating the tessellation. They present an adjusted model, named *Half-Gilbert Tessellation*, for which they derive an analytical expression of the density of the line length. Main techniques used in their work are mean-field analysis and stopping-set theory for Poisson processes.

The definition of the Half-Gilbert model is the key for making their model tractable. In the Half-Gilbert model, only half of the line blocking effects are assumed. Specifically, only lines growing to the right and downwards block each other, as well as left and upward growing lines. For example, a line growing to the left is not blocked by a line growing downward; they both continue in case of collision. However, if it runs into a line growing upward, it is blocked. An example can be found in Figure 29, which is taken from Figure 1 in [2]. It is demonstrated in that paper that this adjusted model is much more tractable. This is mainly because it is possible to find self-similar areas when analysing the area of threat (which is C_v in our model) and the area of influence (which is D_v in our model) for $\{L_v > t\}$. These two areas are the same in the Half-Gilbert model, unlike here. Additionally, the area of threat lies only on one side of L_v due to only half the blocking

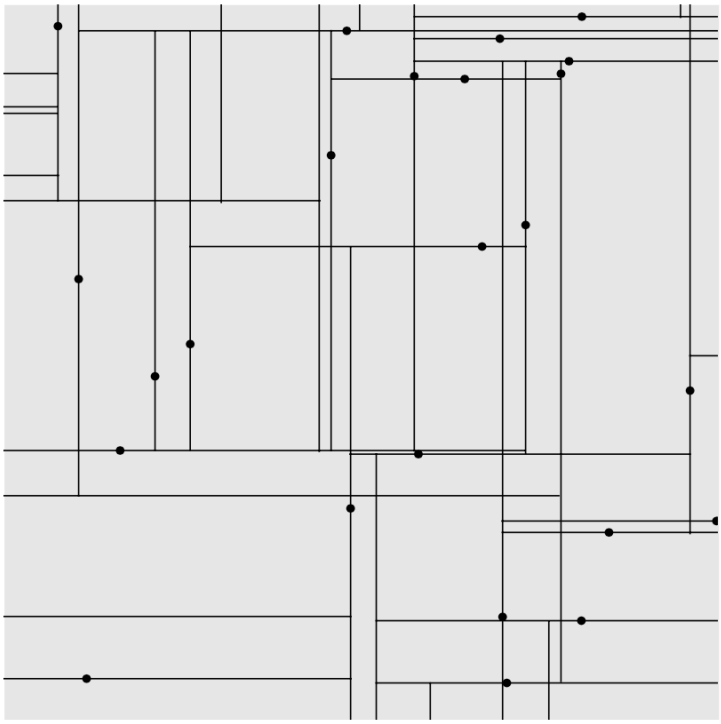

Figure 29: Example of the Half-Gilbert tessellation with equal probability for horizontal and vertical lines. Taken from Figure 1 in [2].

effects, which prevents the added complexity of interactions between the sides in the Full-Gilbert model as illustrated in Figure 16. Through that, it is possible to obtain recursive results.

The density of L_v, i.e., the line in one direction (called *ray* in their work), is derived analytically for the Half-Gilbert model. Burridge, Cowan, and Ma proceed to show that the density in the Half-Gilbert model with intensity λ and the density in the Full-Gilbert model with intensity $\lambda/2$ are indistinguishable by eye when plotted, but mathematically not exactly the same.

Another key achievement in the work by Burridge, Cowan, and Ma is the development of an algorithm which makes it possible to simulate the Full-Gilbert tessellation much more efficiently, and thus faster, than their "obvious" method. With that, they obtain an estimated expected value for L_v from 10^9 replicates, which is 1.467535 for $\lambda = 1$ (see (4) in [2]). That is approximately 3.8% larger than the corresponding value from [12]. That is obtained by taking half of the value presented in [12] respectively for the entire $\mathcal{L}_v$.

Two of the authors of [2], Burridge and Cowan, improve the approximations and simplify the analytical solution in 2016 [1]. An analytical expression for the Laplace-transform is derived as well as higher-order moments. The results are only derived on the Half-Gilbert model. However, due to the close relationship of the Half- and the Full-Gilbert model, this is still relevant to our model. That work even generalised some results from [2]. In particular, the authors derive results on an adjusted Half-Gilbert model,

which allows the lines to grow in other (and possibly more than two) directions than solely vertical and horizontal.

Now that the results are summarised, there are some points for discussion. Considering the scaling relationship of the models with different intensities λ in (136), we disagree with [2], where it is stated at the beginning of Section 3 that $\mathbb{P}(L_{v,\lambda} > t) = \mathbb{P}(L_{v,1} > \sqrt{2\lambda}t)$. Note that here, the size of the box is omitted in the index as the authors work on the entire $\mathbb{R}^2$, but the statement can be used in the same way. We believe that the factor $\sqrt{2}$ is incorrectly used, given the explanations behind (136).

The authors of [2], Burridge, Cowan, and Ma, disagree with the authors of [12], Mackisack and Miles, on the question whether the growths of the lines in opposite directions from one vertex are independent or not. Mackisack and Miles claim that they are not entirely independent but "reasonably independent", without naming reasons, while Burridge, Cowan, and Ma argue that they are independent. Their argument is the same as the one presented in our work, which is that they are independent because the areas in which points can influence the growth of the two lines are disjoint, except for the vertex in question of course (see Figure 14). Additionally, the Poisson process has independent increments, which, together with the former argument, implies independence. Only in our work there is a small dependence, as mentioned in Section 3, due to the finite size of the box (as one of the lines cannot possibly grow further than $N/2$). Since the named publications are based on $\mathbb{R}^2$ and hence do not have this restriction, we agree with Burridge, Cowan, and Ma.

As all three publications work on the entire $\mathbb{R}^2$ rather than a finite square as we do, the question around the (number of) escaping lines is not posed at all and a novelty in this work. This is also true for the covariance, which is not discussed in any of the publications. However, it can be assumed that sharper bounds for the exponential decay can be obtained through the approximations based on results in [1],[2]. Our work is also the only work that presents distributional results on the Full-Gilbert model by providing bounds that hold exactly.

Any exact results on the expected value or distribution of the line length that are not bounds are still not known. The bounds provided in this work and the approximations from [1], [2], [12] provide more insight and can lead to further progress on this question.

There are many more ways to generalise the model presented here. One way would be to change the Poisson process into other point processes. For example, one could take away the homogeneity, meaning the intensity of the Poisson process is not identical on all of Ω. One could also allow for covariance structures within the point process. The generalisation presented in Section 5.2 clearly leads to the original Gilbert tessellation when removing the finiteness of the considered area.

References

[1] J. Burridge and R. Cowan, "Planar Tessellations that have the Half-Gilbert Structure," *Advances in Applied Probability*, volume 48, number 2, 574–584, 2016. DOI: 10.1017/apr.2016.15.

[2] J. Burridge, R. Cowan, and I. Ma, "Full- and Half-Gilbert Tessellations with Rectangular Cells," *Advances in Applied Probability*, volume 45, number 1, 1–19, 2013. DOI: 10.1239/aap/1363354100.

[3] S. N. Chiu, D. Stoyan, W. S. Kendall, and J. Mecke, *Stochastic Geometry and its Applications* (Wiley Series in Probability and Statistics). John Wiley Sons, 2013. DOI: 10.1002/9781118658222.

[4] H. Ekström and T. Turova, "Non-monotone Cellular Automata: Order Prevails over Chaos," *BioSystems*, volume 220, 2022. DOI: 10.1016/j.biosystems.2022.104756.

[5] P. Erdős and A. Rényi, "On Random Graphs I," *Publicationes Mathematicae Debrecen*, volume 6, pages 290–297, 1959.

[6] E. N. Gilbert, "Random Graphs," *The Annals of Mathematical Statistics*, volume 30, number 4, 1141–1144, 1959. DOI: 10.1214/aoms/1177706098.

[7] E. N. Gilbert, "Surface Films of Needle–Shaped Crystals," *Applications of Undergraduate Mathematics in Engineering*, B. Noble, Ed., pages 329–346, 1967.

[8] G. Grimmett, *Percolation* (Grundlehren der mathematischen Wissenschaften). Springer-Verlag Berlin Heidelberg New York, 1999, volume 321. DOI: 10.1007/978-3-662-03981-6.

[9] A. Gut, *An Intermediate Course in Probability* (Springer Texts in Statistics). Springer New York, NY, 2009. DOI: 10.1007/978-1-4419-0162-0.

[10] M. Harchol-Balter, *Introduction to Probability for Computing*. Cambridge University Press, 2023. DOI: 10.1017/9781009309097.

[11] G. Last and M. Penrose, *Lectures on the Poisson Process* (Institute of Mathematical Statistics Textbooks). Cambridge University Press, 2017. DOI: 10.1017/9781316104477.

[12] M. S. Mackisack and R. E. Miles, "Homogeneous Rectangular Tessellations," *Advances in Applied Probability*, volume 28, number 4, pages 993–1013, 1996. DOI: 10.2307/1428161.

[13] M. Mitzenmacher and E. Upfal, *Probability and Computing: Randomized Algorithms and Probabilistic Analysis*. Cambridge University Press, 2005.

[14] H. Teicher, "An Inequality on Poisson Probabilities," *The Annals of Mathematical Statistics*, volume 26, pages 147–149, 1955. [Online]. Available: https://www.jstor.org/stable/2236771.

[15] E. Wolfstetter, "Stochastic Dominance: Theory," in *Topics in Microeconomics: Industrial Organization, Auctions, and Incentives*. Cambridge University Press, 1999, 135–148. DOI: 10.1017/cbo9780511625787.005.

Master's Theses in Mathematical Sciences 2024:E21
ISSN 1404-6342

LUNFMS-3126-2024

Mathematical Statistics
Centre for Mathematical Sciences
Lund University
Box 118, SE-221 00 Lund, Sweden

http://www.maths.lu.se/